Research Paper

ER-depletion lowering the 'hypothalamus-uterus-kidney' axis functions by perturbing the renal ERβ/Ptgds signalling pathway

Yan-Ru Liu[1,*], Zhi-Shu Tang[1,*], Jin-Ao Duan[2], Lin Chen[1], Jing Sun[1], Rui Zhou[1], Zhong-Xing Song[1], Xin-Bo Shi[1], Hui-Yuan Zhu[3]

[1]Shaanxi Province Key Laboratory of New Drugs and Chinese Medicine Foundation Research, Shaanxi Collaborative Innovation Center of Chinese Medicinal Resources Industrialization, Shaanxi University of Chinese Medicine, Xianyang 712083, P.R. China
[2]Key Laboratory for High Technology Research of TCM Formulae and Jiangsu Collaborative Innovation Center of Chinese Medicinal Resources Industrialization, Nanjing University of Chinese Medicine, Nanjing 210023, P.R. China
[3]Shaanxi University of Chinese Medicine, Xianyang 712083, P.R. China
*Equal contribution

Correspondence to: Jin-Ao Duan, Yan-Ru Liu; **email:** dja@njutcm.edu.cn, yanzi_2203@aliyun.com
Keywords: estrogen receptor beta, 'hypothalamus-uterus-kidney' axis, prostaglandin D_2 synthase, menopause
Received: June 6, 2019 **Accepted:** October 26, 2019 **Published:** November 10, 2019

ABSTRACT

Researchers have long assumed that systematic estrogen fading might contribute to the sustained progression of menopausal degenerate syndromes, although definitive evidence has not been presented. Whether such findings represent a causal contribution or are the result of opportunistic messengers sent from the reproductive system to the brain is also a vital question. We constructed a multiscale network of the ovariectomy (OVX) induced estrogen receptors depletion (ER-depletion) model and integrated targeted proteomic, targeted lipidomic, cytochemical, and histopathological data across three tissues from the ovariectomy rodent model. We found that compared to control rats, OVX rats showed increased renal and uterine prostaglandin D2 synthase (Ptgds) expression and decreased hypothalamic Ptgds expression, abnormal Ptgds metabolites, the degenerate renal function profiles and decreased cognitive ability (learning and memory) in Morris water maze test. Importantly, we observed a regulatory relationship among ER (particularly ERβ), the degree of the pathological phenotype, learning behavior test and the 'hypothalamus-uterus-kidney (HUK) axis functions. Collectively, this study elucidates that ER depletion promoted HUK aging is mostly attributed to a renal ERβ/Ptgds signalling imbalance.

INTRODUCTION

Female ageing begins with the ageing of the reproductive system, which drives primordial follicular ovarian pools to accelerate consumption. Accompanied by estrogen depletion and turbulence, menopausal ovarian failure is the final step in this process [1]. Menopause, an inevitable stage of ageing among 45~55-year-old women, is a complex process involving a variety of cellular and molecular changes. Menopause has been described to have different "appearances"; the main physiological manifestations are ovary fading and suffering from various phenotypic syndromes, such as hot flashes, anxiety, insomnia, depression, osteoporosis, and cognitive decline [2]. In addition to the typical symptoms of these menopausal syndromes, there is actually a symptom of rapid ageing. The emergence of rapid ageing is partially due to age, and rapid ageing has a very important relationship with the loss of estrogen in menopause.

Data from epidemiological studies show that menopausal women have a higher risk to develop chronic kidney disease (CKD) [3]. These conditions will not occur spontaneously in the same individual but may subsequently lead to related neurological diseases. Patients with kidney small vessel disease, endothelial dysfunction, and increased oxidative stress are prone to CKD, which induces cognitive impairment in patients [4]. A higher prevalence ranging from 16% to 38% of cognitive decline is related to CKD and increases the risk of mortality [5]. Due to a lack of updated guidelines or commentary for menopausal women with clinical nephrological diseases, research about the relevance of ovarian failure-induced estrogen loss on CNS dysfunction and the mechanistic links between the dysfunction of the kidney and brain also needs to be conducted. Considering previous results, we found that many menopause symptoms are significantly associated with elevated renal toxicity markers [6]. The results of these documents are suggestive of a nephrology contribution to menopausal degenerate function, though reports offer little insight into promising mechanisms, and a consistent relationship with specific renal genes has not been explored. Therefore, before revealing the ovarian failure response to the HUK axis, understanding and exploring the relationship between the effects of menopausal oestrogen and kidney disease is more essential. Since estrogen binds to nuclear estrogen receptors to alter the expression of many genes in the modulation of the body's systemic metabolism, it is necessary to identify estrogen response genes and to explore their binding interactions before evaluating the risks of estrogen loss on organs in menopause. Certainly, it is unrealistic to explore how the multiple genes and their signalling pathways act on organs in a parallel way. Recent findings have indicated that a higher prevalence of renal lipotoxicity was observed among a menopausal CKD group. As an important factor in the development of impaired renal function in menopausal women, lipotoxicity can stimulate chronic inflammation and exacerbate oxidative stress. As pro-inflammatory adipose tissue macrophages (ATMs) accumulate, the resultant lipid imbalance may trigger macrophage infiltration and pro-inflammatory cytokine production, thus leading to local fat cell dysfunction [7].

Here, we conducted this study to draw and match biological networks underlying two distinct menopausal-related phenotypes via multiple independent datasets collected from rodents. We assumed that a multiscale network of ovariectomized (OVX) models would provide fresh insight into the molecular endocrinology context without clinical symptoms [8]. By using OVX rats as a model of systemic disruption, we began with a computational characterization of a specific endophenotype of menopause. Then, we directly enriched specific genes and metabolites in a multiscale network calculation of multiomic datasets together with biochemistry, histopathology, immunohistochemistry, Western blotting, and mRNA sequencing data. The exhaustion of the female reproductive system and the kidney function alterations with fluctuating levels of lipid metabolic genes affects the systemic metabolism. This study maps a 'disease phenotypes-genes- metabolites' network to explore whether ER-depletion induced renal profile disturbing results in brain dysfunction. The study design offers novel evidence in a data-driven approach to link renal lipid-gene distortion in menopause period, which facilitates the integration of diverse biomedical data with multiple disease stages. Our results provide evidence of renal gene perturbations in menopausal degenerative diseases, particularly involved in lipid metabolism pathways. In summary, these data provide compelling evidence linking the relationship between ER-depletion with renal lipid gene along the 'Hypothalamus-uterus-kidney' axis after ovarian failure.

RESULTS

OVX-induced ER-depletion promotes distinct proteomic signalling outcomes

The experimental protocol was shown in Figure 1 (Study design). Since the proteome provides extensive information on the molecular mechanisms that regulate the cellular events between genotypes and their phenotypic manifestations [9]. To understand the underlying ovarian failure induced ER-depletion process on systemic function, we performed an isobaric tags for relative and absolute quantification (iTRAQ)-based proteomics analysis on urine samples from control (sham) and ovariectomized (OVX) rats.

Among the global proteins in the rat proteome, 251 proteins were quantified. We then selected differentially expressed proteins based on the cut-off conditions of a 1.5-fold change and a p value < 0.05. As a result, 55 proteins were identified to be highly related and differentially expressed, with 25 upregulated and 30 downregulated proteins, triplicate analysis was performed (Figure 1A, Supplementary Table 3).

Ingenuity pathway analysis (IPA) identified 'Neurological Disease' (p = 3.61E-09 to 4.26E-03, 22 proteins), 'Reproductive System Disease' (p = 1.23E-04 to 2.98E-03, 20 proteins), 'Metabolic Disease' (p = 1.52E-04 to 4.26E-03, 17 proteins), 'Renal and Urological System Development and Function' (p = 1.56E-04 to 1.86E-03, 4 proteins), and 'Renal and Urological Disease' (p = 4.59E-04 to 2.13E-03, 5

proteins) (Supplementary Table 4) as the most significant disease categories. Interestingly, within these categories, the most significantly associated upstream regulator term was 'beta-estradiol' (p = 1.06E-08), which was associated with ovarian failure-induced abnormalities. Notably, organic toxicity functions were most significantly associated with 'Acute Renal Failure Panel' (p = 9.18E-06, 4 proteins), 'Long-term Renal Injury Antioxidative Response Panel' (p = 6.66E-04, 2 proteins), 'Positive Acute Phase Response Proteins' (p = 1.86E-03, 2 proteins), and 'Persistent Renal Ischemia-Reperfusion Injury' (p = 1.86E-03, 2 proteins) (Supplementary Table 5). These proteome changes altered by OVX indicated a dramatic effect on the estrogen regulation and more intensive occurred in kidney.

ER-depletion disturbs the cellular communication in renal microenvironments

All differentially expressed proteins were mapped to various terms in the Gene Ontology (GO) database, and the proteins for each term were counted and calculated by a hypergeometric test and were mapped to the enriched GO terms. GO annotation indicated that the ovarian failure proteome was significantly enriched in the 'Cellular Components of the Extracellular Space', 'Extracellular Exosome', 'Extracellular Space', 'Integral Component of the Membrane', 'Blood Microparticle', 'Nucleus', 'Lysosome', 'Plasma Membrane', 'Cytoplasm', and 'Extracellular Region' (Figure 1B, Supplementary Table 3). In particular, many secreted proteins were annotated as 'Extracellular Exosomes' (28 proteins, including 14 upregulated and 14 downregulated proteins) or 'Extracellular Space' (22 proteins, including 10 upregulated and 12 downregulated proteins) (Figure 1C, 1D, Supplementary Table 3). Notably, among these abnormally expressed proteins, 19 proteins were reported as kidney disease markers (Ada, Ambp, Anxa1, B2m, Camp, Col1a1, Cp, Ggt1, Glb1, Lgfbp7, Lifr, Lpl, Plau, Ptgds, S100a8, Serpinc1, Serpina3k, Tff1, and Vtn) [10–25] (Supplementary Table 3, highlight in green). These data suggest that ER depletion mainly interferes renal proteins' extracellular communication.

ER-depletion alters renal lipid molecular transport functions

According to IPA disease categories, molecular function (MF) and biological process (BP) enrichment of these 19 renal-specific proteins exhibited major lipid metabolism (4.41E-06 to 4.09E-03, 5 proteins, Supplementary Table 6), including calcium ion binding (Anxa1, S100a8) lipoprotein particle receptor activity (Lpl), prostaglandin-D synthase activity (Ptgds), acyl-glycerol metabolic process (Lpl), neutral lipid metabolic process (Lpl), response to lipopolysaccharide (S100a8, Plau, Serpina1,), response to corticosteroid (Col1a1, Anxa1, Ptgds), lipid transport (Anxa1), fatty acid biosynthetic process (Anxa1, Ptgds, Lpl), response to glucocorticoid (Ptgds, Anxa1), and lipid localization (Anxa1) involving in7 proteins including Anxa1, Col1a1, Lpl, Plau, Ptgds, S100a8, and Serpinc1 (Supplementary Table 3, highlight in yellow). These 8 proteins, renal-specific proteins annotated in the Human Protein Atlas were significantly dysregulated, revealing that the loss of renal lipid protein is an important overall feature of ovarian failure (Figure 1E). These observations indicate that diminishing ovarian estrogen secretion triggers extensive renal lipid metabolism derangement.

Ovarian failure leads to enrichment of the signalling pathways associated with ERβ-regulated cell-to-cell signalling and renal lipid metabolism

Network analysis returned three correlation networks linking all of the differentially regulated proteins with an IPA p-score (IPA p-score = −log10 [p value]), including 'Cellular Movement, Haematological System Development and Function, Immune Cell Trafficking' (IPA p-score = 42, 18 proteins), and 'Cell-To-Cell Signalling and Interaction, Carbohydrate Metabolism, and Lipid Metabolism' (IPA p-score = 11, 7 proteins). Consistent with the results of the previous analysis, eight proteins implicated in renal lipid metabolic disease have been highlighted to be associated with the network, including upregulated Ptgds, Ambp and downregulated Anxa1, Camp, Col1a1, Lifr, and Myh6 (Supplementary Tables 7 and 8).

We then further examined the eight proteins' relationships with estrogen regulation and explored the proteins with the greatest impacts on ovarian failure using the GeneMANIA platform. All eight proteins were subjected to leading edge analysis by physical interactions, shared protein domains, and co-localization. The weighted results showed that the six terms that were most significantly associated with the biological process closely related to estrogen-regulated renal lipid metabolism at a cut-off FDR < 10% were 'Response to Estrogen', 'Response to estradiol', 'Triglyceride Metabolic Process', 'Response to Glucocorticoid', 'Response to Corticosteroid', and 'Enzyme Inhibitor Activity' (Figure 1F, Supplementary Table 9). Meanwhile, we found a close co-expression correlation among ERβ, Ambp, Ptgds, Anxa1, and Col1a1 in the network.

Furthermore, Kyoto Encyclopedia of Genes and Genomes (KEGG) enrichment from MetaboAnalyst platform (http://www.metaboanalyst.ca) [26] returned

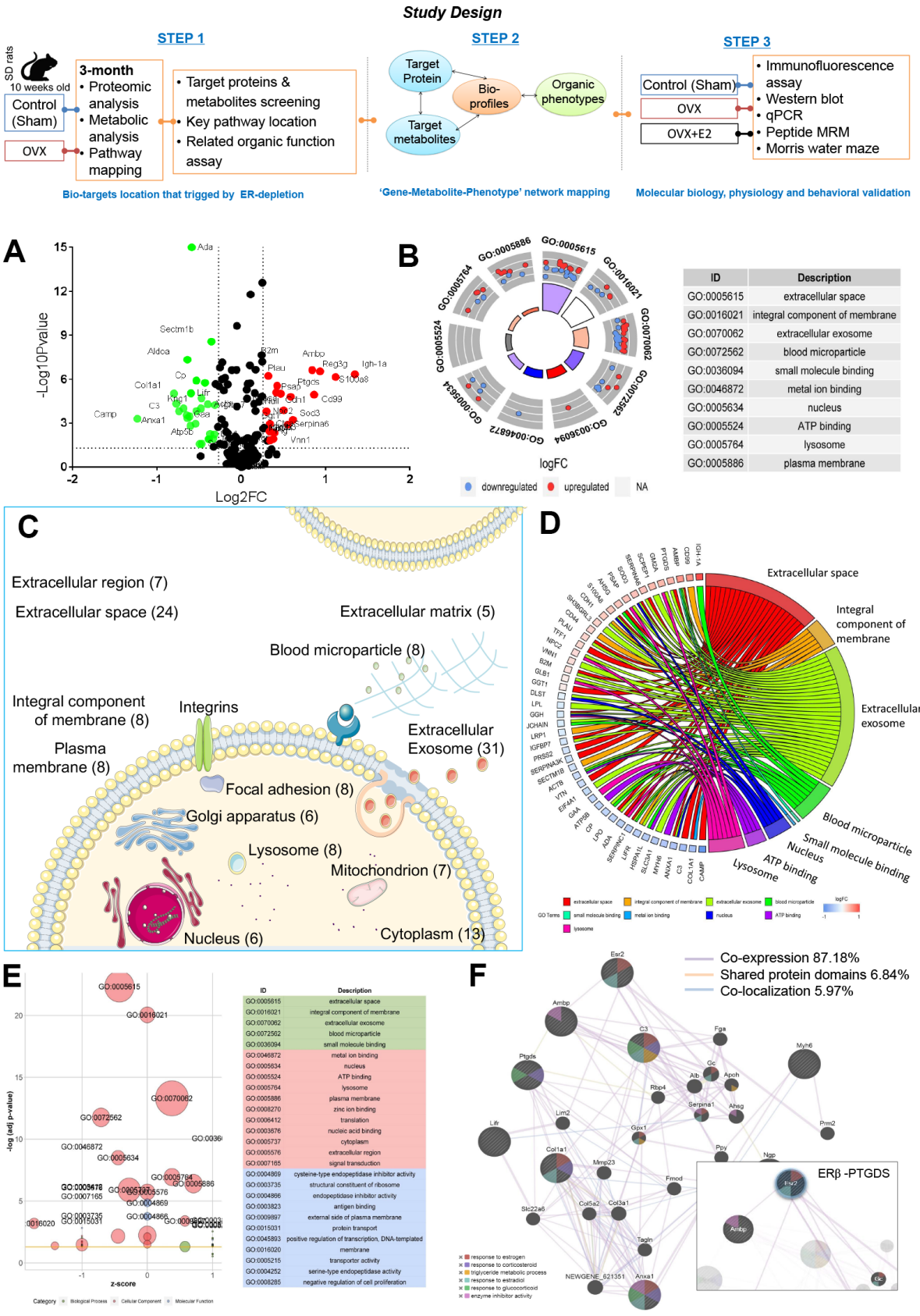

Figure 1. Ovarian failure induced overall proteomic regulation dysfunction as shown by proteomic analysis. (**A**) Volcano plot of differential proteins screened between control and OVX rats (normalized by control sample data). (**B**) GO Circle plot for significant

enrichment of cellular components (CC) for genes that are strong candidates for ovarian failure-induced dysfunction. (**C**) Subcellular locations of ovarian failure proteins annotated by Gene Ontology. (**D**) GO-Chord plot illustrating the gene-annotation enrichment relationships and representative significant GO terms that are distinctly classified into species-specific gene clusters. (**E**) GO-Bubble plot illustrating significant enrichment of molecular functions and biological processes (adjusted p-value < 0.05) and the z-score of the term (**F**) Protein–protein interaction network identified using GeneMANIA (direct interaction database).

two metabolism pathways including 'Arachidonic acid (AA) metabolism' (p=0.003, path: rno00590, Ptgds, Ggt1), and 'Taurine and hypotaurine metabolism' (p=0.009, path: rno00430, Ggt1). In line with the KEGG annotation, Ptgds was highlighted as being associated with the lipid metabolism networks (Supplementary Table 10). These findings suggest that the gene association sets of ERβ/Ptgds singling pathway may have close relationships with lipid synthesis, transfer, and metabolic signalling between extra- and intracellular membranes.

Urinary and serum eicosanoid disturbances reflect lipid metabolism disorder

Eicosanoids in arachidonic acid metabolism are key metabolites in the aetiology of metabolic syndrome (MetS), we next investigated whether the eicosanoid perturbation in rats with ovarian failure was due to the ER-depletion and defects in renal absorption. Therefore, we measured local metabolites in the kidney by metabolome analysis (Supplementary Figure 2).

PLS (partial least-square) analysis from MetaboAnalyst platform of the metabolome showed a distinct change in the metabolite profiles in the kidneys of rats with ovarian failure 12 weeks after ovariectomy relative to those of the age-matched control rats as represented by substantial eicosanoids distortion in the urinary system (three experiments, Figure 2A). Here, significant features were selected based on a specific criterion with a cut-off adjusted p value < 0.05, a fold change > 1.5, and an AUC > 0.75 for each dataset (Figure 2B). Statistical analysis of the metabolomics data from the OVX and control rats revealed statistically significant differences in ions between these two groups, as shown in the volcano plot (Figure 2C). Average variable importance in projection (VIP) scores was also used to calculate feature importance with a VIP score > 1. After meta-analysis selection, 22 and 13 of 155 eicosanoids in the urine and serum, respectively, were identified as potential biomarkers for arachidonic acid metabolism evaluation (Figure 2D, Supplementary Tables 3, 11 and Supplementary Figure 1). Pathway enrichment analysis of the KEGG database indicated that these 35 eicosanoid markers were mostly involved in the following three metabolic pathways: AA metabolism, biosynthesis of unsaturated fatty acids, and linoleic acid metabolism (Figure 2E).

Pathway enrichment analysis detected that the most significant differences between the OVX rats and the control rats were related to prostaglandins. As major products of AA generated from mast cells, the physiological importance of prostaglandins is illustrated by the numerous diseases to which these abnormalities contribute, including inflammatory diseases, diabetes, obesity, and cancer. The abundant prostaglandins in urine that exhibited rapid decreasing trends included 15d PGD_2, dhk PGD_2, PGJ_2, dihomo PGJ_2, 20oh PGE_2, PGA_2, PGB_2, and 8-iso PGF_{3a}, whereas AA, PGF_{2a}, 15k PGF_{2a}, 11bdhk PGF_{2a}, PGFM, and 6kPGF_{1a} showed increasing trends. Moreover, a significant reductions in the levels of prostaglandins in the serum, such as 15k PGE_2, 8-iso PGF_{3a}, dhk PGF_{2a}, PGJ_2, PGB_2, 15k PGD_2, and 15d PGJ_2, as well as the depletion of the unsaturated fatty acids AA, docosahexaenoic acid (DHA), and eicosapentaenoic acid (EPA) (Figure 2F, 2G; Supplementary Table 11). These prostaglandin alteration trends, which correspond to the proteomic data, also indicated weakened adipose cell transportation in rats with ovarian failure induced ER-depletion, which attenuates renal lipid metabolism and ultimately promotes local lipid accumulation.

The 'Gene-Metabolite-Phenotype' network revealed ER-depletion trigger Ptgds abnormal expression and perturbs HUK axis functions

To study complex ER-depletion induced metabolism disease and to gain systemic functional insights, we evaluated Ptgds activity in a multiscale network analysis via SIMCA-p (version 14.0, Umetrics, Umeå, Sweden) of four datasets containing organic phenotype datasets, organic function datasets, key protein datasets, and metabolomic datasets.

Ptgds is a clinical diagnostic marker that is expressed on the extracellular membranes of tissues and fluctuates in body fluids under various pathological conditions; in addition, this marker is essential for the generation of various prostanoids with numerous physiological and pathophysiological functions. We performed MRM-based targeted proteomics analysis by measuring the ratio of heavy-isotope-labelled peptides in urine samples by LC-MS in MRM mode, we observed that the Ptgds levels were significantly higher in the OVX rats than in the control rats. (Figure 3A, Supplementary Table 12). Since Ptgds promoter activity was mainly modulated by ERβ, which is consistent with the high

expression pattern observed for uterus ERβ in the cardiovascular, reproductive, and urinary systems (the brain, heart, ovaries, and kidneys). We performed real time polymerase chain reaction (PCR) analysis for ERβ assay (ref. NM_012754.1, 204 bp, 60°C, Servicebio: forward primer: 5′- CTGGGTGATTGCGAAGAGT GG -3′ and reverse primer: 5′- GAGGACTTGTA CCCTCGAAGCG -3′) (Figure 3B, Supplementary Table 11).

The body weights were monitored weekly, and organic morphological changes were assessed at 3-month intervals. The average weekly body weights were significantly higher in the OVX rats compared to the control rats. In contrast, the OVX rats displayed a significant deterioration of their organ/body weight ratios (heart, liver, spleen, lung, kidney, uterus, brain, hippocampus, and hypothalamus), demonstrating that ovariectomy accelerates organic tissue deterioration (Figure 3C, Supplementary Table 12).

We next assessed whether reduced ovarian function in the OVX rats had an effect on the biochemical profiles (kidney profile and lipid profile). For the kidney profile (organic function), all OVX rats presented a higher levels of serum albumin (ALB), uric acid (UA), urea, glucose (GLU), and creatinine levels compare to control rats (Figure 3D, Supplementary Table 12). For the lipid profile, increasing trends for the levels of TC, TGs, and LDL were observed, while a decreasing trend was observed for the HDL level in the OVX group (Figure 3E, Supplementary Table 12). These results revealed a relationship between renal lipid metabolism dysfunction and ovarian failure induced ER-depletion.

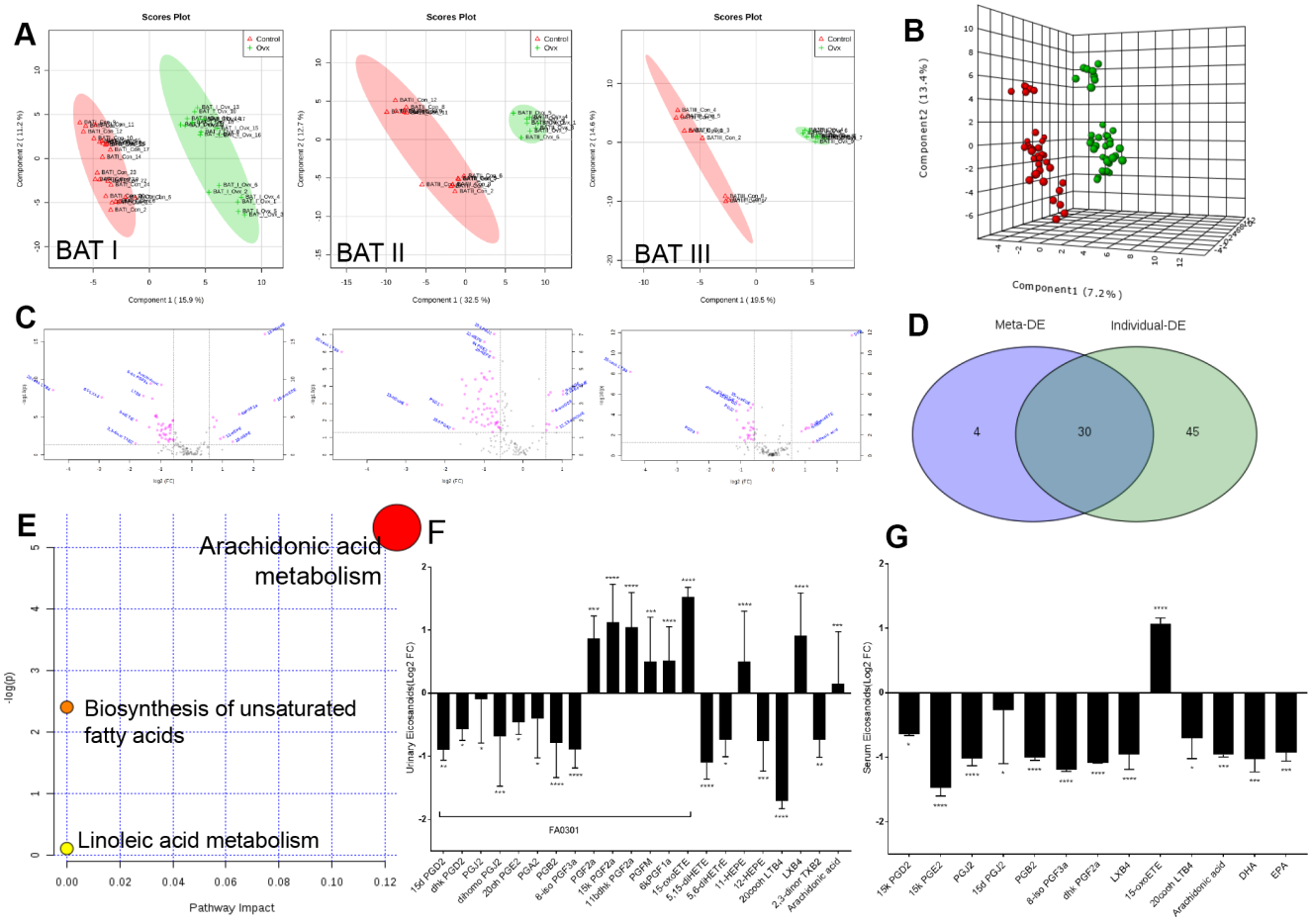

Figure 2. Imbalances of eicosanoids in the kidneys of OVX rats. (**A**) PLS analysis of the metabolome profile of the kidney in the control and OVX rats from three experiments. (**B**) Meta-analysis and PLS analysis of urinary eicosanoids in control rats (n = 45) and OVX rats (n = 45). (**C**) Volcano plot for eicosanoid changes with pink colour reflecting decreases/increases. (**D**) Venn diagram of the top differentially expressed features from the meta-analysis. (**E**) Pathway enrichment plot of the biomarkers in each pathway. (**F**) Liquid chromatography–tandem mass spectrometry analysis of eicosanoids (Log2 FC) from urine samples. (**G**) Liquid chromatography–tandem mass spectrometry analysis of eicosanoids (Log2 FC) from serum samples. n=6, mean ± s.d., compared to control rats, *p < 0.05, **p < 0.005, ***p < 0.0005 and ****p < 0.0001.

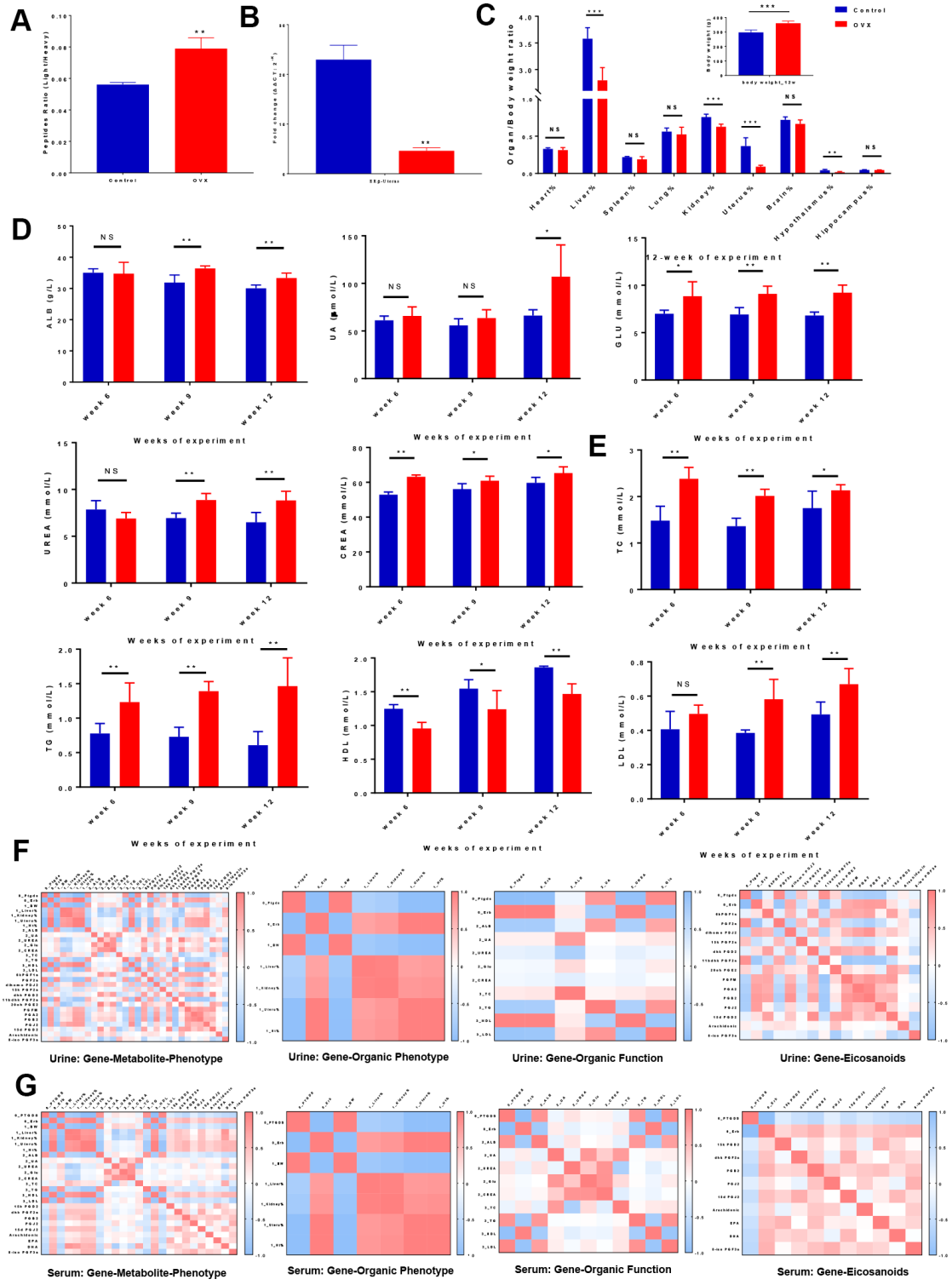

Figure 3. Correlation analyses illustrated the relationships among 'genes-metabolites-phenotypes' in ER-depletion-induced renal lipid metabolism disorder. (**A**) Relative peptide quantification in control and OVX rat urine samples. n=3, mean ± s.e.m.; (**B**) Real time PCR assays of uterus ERβ among control, OVX and OVX+E2 rats. n=3, mean ± s.e.m.; (**C**) Average weekly body weight (g) from 0 to 12 weeks before and after surgery and average organ/body weight ratio (organ %) at 12 weeks after surgery. (**D**) Kidney biochemical profiles in the sera of control and OVX rats. (**E**) Lipid biochemical profiles in the sera of control and OVX rats. n=6, mean ± s.d., compared to control rats, *$p < 0.05$, **$p < 0.005$, ***$p < 0.0005$. Correlation heat map representation of the differentially expressed gene and metabolite markers in organs, renal biochemistry, and lipid biochemistry phenotypes including genes clustered into organ phenotypes, subsets of genes clustered into organ functions and subsets of genes clustered into eicosanoid markers in urine (**F**) and serum (**G**).

For multiscale evaluation, we analysed each set of omics data individually and then combined the 'diseases-genes-metabolites' to generate a 'big picture'. By integrating the power of networks and evidence-based biological knowledge, the selected biomarkers (i.e., genes, metabolites, and phenotypes) were co-projected onto the networks to reveal important links among ovarian failure, ER-depletion, renal lipid metabolism, and other organs` diseases. We investigated whether strong Ptgds inhibition had a systematic effect on the body phenotypes (body weight and organic ratios) and organic functions (biochemistry parameters). 'Gene-to-Gene' correlation analysis showed a highly significant negative correlation between uterine ERβ and urine Ptgds, indicating that renal Ptgds overexpression caused by ovarian failure is mainly regulated by ERβ. We investigated whether strong Ptgds inhibition induced by ER-depletion had a systematic effect on the body phenotypes (body weight and organic ratios) and organic functions (biochemistry parameters). Accordingly, 'Gene to Organic Phenotypes' and 'Gene to Organic Function' correlation analyses showed that ERβ depletion was highly correlated with kidney and uterus organic phenotypes (kidney % coef.: 0.804, uterus % coef.: 0.999). Notably, urine Ptgds was highly correlated with kidney function (kidney % coef.: -0.804 and ALB coef.: 0.817) and lipid metabolism (body weight coef.: 0.979, TG coef.: 0.820, HDL coef.: -0.965, and LDL coef.: 0.921). However, uterus ERβ had the opposite correlation with kidney dysfunction and lipid metabolism disorder compared with those of urine Ptgds. (Figure 3F, 3G, Supplementary Table 13).

We further investigated whether the fluctuation of eicosanoid dynamics was due to Ptgds overexpression that suffered from ER-depletion. Thus, we next performed a correlation analysis on the 'Gene to Eicosanoids' relationship and showed that ERβ depletion was highly correlated with the Ptgds-catalysed urinary PGF_{2a} (coef.: 0.889), 11bdhk PGF_{2a} (coef.: 0.858), PGJ_2 (coef.: -0.768), dihomo PGJ_2 (coef.: -0.654), PGA_2 (coef.: -0.738), PGB_2 (coef.: -0.782), serum PGB_2 (coef.: -0.602), and 15d PGJ_2 (coef.: -0.503) levels.. In addition, PGJ_2, 15d PGJ_2, and dihomo PGJ_2 were produced from PGD_2 in the arachidonic acid pathway [26, 27]. These PGD_2 derivates exhibit the opposite effects on the glucose homeostasis and adipocyte differentiation involved in kidney diseases; therefore, the relationship between the diminished amount of PGD_2 derivates in bio-fluids and the overexpressed tissue-specific Ptgds indicated that these PGD_2 derivates elicit their lipid toxicity stimulated by accumulating in extracellular space (Figure 3F, 3G, Supplementary Table 13). These data indicate that the ovarian failure induced accelerated degradation of ERβ in rats cause Ptgds overexpression in the kidney, and possibly altered the systemic lipid metabolism disorder resulting in HUK axis degenerative changes.

Immunofluorescence (IF), Western blot (WB), real time polymerase chain reaction (PCR) assays and Spatial learning behavior test confirmed that ER-depletion reduce HUK functions attribute to ERβ/Ptgds signalling pathway disturbance

To further confirm how the ER-depletion disturbing ERβ/Ptgds signalling pathway and reducing HUK function, a subset of OVX rats were administered E2 therapy (Figure 1, Study design), and IF, WB, PCR assays and spatial learning behavior test (Morris water maze test) were performed. In the IF analysis, double staining was conducted that red colour present ERβ and green colour present Ptgds. The AOD ratio indicates the ratio of optical density (IOD) and values to staining area (AREA), that a larger AOD ratio represents a higher protein expression level. As expected, ERβ was specifically localized in nucleus, Ptgds localized in cellular membrane or extracellular space. Compared to those of the control rats, OVX rats showed a weak ERβ signal in kidney, uterus and hypothalamus. Kidney from OVX rats showed strong Ptgds signal in tubules but had a dimished signal in uterus and hypothalamus (Figure 4A–4C). E2 therapy significantly restored the ERβ/Ptgds staining AOD scores in hypothalamus, uterus, and kidney (both the overexpressed protein and the control) (Figure 4D, Supplementary Table 14).

We next assessed the effects of ER-mediated marker genes as well as the antagonism of kidney function by WB assays. ERβ expression was significantly decreased in the kidney, uterus and hypothalamus of the OVX rats. More importantly, a sharp increase in Ptgds expression was observed in OVX rat kidneys compared to the control rats; however, decreased Ptgds expression was identified in the uterus and hypothalamus (Figure 4E–4G). All the parameters were rescued by E2 treatment (Figure 4H, Supplementary Table 14). In agreement with these results, PCR analysis for expression comparison in the same tissues indicated a significant decline in the mRNA level of ERβ in the kidneys, uterus, and hypothalamus after ovarian failure that had been rescued by E2 therapy (Figure 4I–4K, Supplementary Table 14). Ptgds expression in the kidneys was increased in OVX rats but was restored by E2 treatment (Figure 4I). Specifically, ovarian failure reduced the relative expression of uterus and hypothalamus Ptgds, while E2 therapy completely reversed the changes (Figure 4J, 4K). In a location test of Morris water maze test, which measures spatial learning activity that were associated with hypothalamus function, OVX rats showed decreased learning and recognize activities (increased escape latency duration and swimming length) compared to that

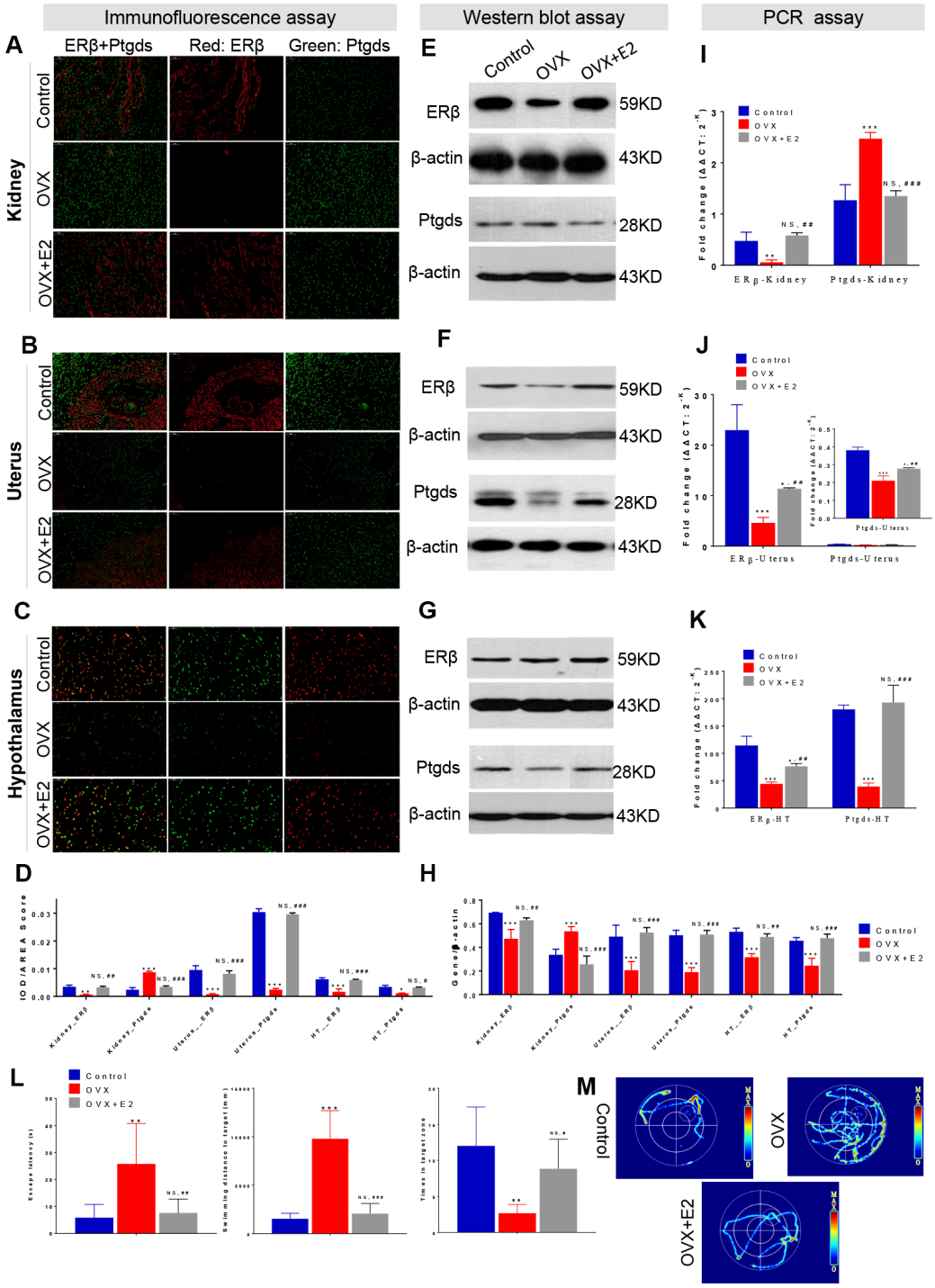

Figure 4. ER-depletion reduce HUK functions attribute to ERβ/Ptgds signalling pathway disturbance. Immunofluorescence (IF) analysis including the staining images (**A**–**C**) and AOD calculation data (**D**) in the left panel shows the double staining of ERβ (red) and Ptgds (green) from kidney (**A**), uterine (**B**), and hypothalamic (**C**) among control, OVX, and E2+OVX rats. Scale bar, 50 μM. The AOD ratio indicates the ratio of optical density (IOD) and values to staining area (AREA). Western blot (WB) analysis including the gel images (**E**–**F**) and protein loading data (**H**) in the middle panel present the ERβ and Ptgds proteins expression from kidney (**E**), uterine (**F**), and hypothalamic (**G**) among control, OVX, and E2+OVX rats. n=3, mean ± s.e.m. Real time PCR analysis of the transcription levels of ERβ and Ptgds expression various among control, OVX and OVX+E2 rats along 'hypothalamus-uterus-kidney axis' in the right panel (**I**–**K**). n=3, mean ± s.e.m., NS, not significant. Morris water maze test including location test and spatial learning test for control, OVX, and E2+OVX rats. As well as (**L**) escape latency duration, swimming length to the escape platform, number of crossings escape platform position, and (**M**) the images of total movement towards to the target for control, OVX, and E2+OVX rats. n=6, mean ± s.d., *p < 0.05, **p < 0.005, ***p < 0.0005 versus control rats; #p < 0.05, ##p < 0.005, ###p < 0.0005 *versus* control rats, NS, not significant.

of control rats. While E2 treatment rats generally spent less time to search the escape platform and reduced distance of travel than did OVX rats. There were no significant differences between the groups of control and E2 treatment rats (Figure 4L, Supplementary Table 14). In addition, in a spatial learning test of Morris water maze test, OVX rats exhibited a decline memory activity (reduced number of crossings escape platform position) than were control rats. No difference between control rats and E2 treatment rats was observed (Figure 4M, Supplementary Table 14).

Overall, E2 restoration effect indicated the relationship of ERβ/Ptgds signaling pathway. These data further confirmed that the upstream ERβ depletion activated renal Ptgds overexpression resulting renal lipid metabolism imbalance, decreased Ptgds transportation to hypothalamus and possibly continuing accelerate HUK function degeneration.

DISCUSSION

In the past decade, scientific reports have shown that urinary Ptgds contributes to renal failure progression. Moreover, ERβ has been reported to stimulate Ptgds expression in female rat hearts; in addition, the engagement of the ER on Ptgds estrogen response elements (EREs) is essential for the acquisition of effector function, and the duration and strength of acute and chronic estrogen responses on Ptgds EREs are related to the integration of co-receptor signals [28]. As a member of the lipocalin family, Ptgds catalyses PGH_2 isomerization into PGD_2 and transports small hydrophobic molecules to the extracellular space and to various body fluids [29, 30]. Then, PGD_2 is sequentially transformed into PGJ_2 and into 15 deoxy $PG^{\Delta 12,\ 14}$ J_2 ($15dPGJ_2$) [31]. The activation of Ptgds can affect lipid metabolic shifts, such as those of arachidonic acid [32], α-linolenic acid (ALA), and eicosanoid metabolism within the cyclooxygenase (COX) pathway [33, 34]. Ptgds secreted in urine is synthesized in Henle's loop and the glomeruli and is mainly degraded by proteolysis after filtration from glomerular capillaries; then, its N-terminal-truncated form is ultimately excreted in urine [35]. Due to its low molecular weight and anionic properties, Ptgds can more easily pass the renal glomerular capillary wall than can serum albumin and can more accurately reflect changes in glomerular permeability. Indeed, lipid metabolism deficiency has been investigated in lipocalin-type PGD_2 synthase (L-Pgds)-knockout (KO) mice and kidney dysfunction patients, which have a susceptibility to glucose intolerance, accelerated insulin resistance, and aggravated obesity [36, 37]. Although considerable research has explored the role of prostaglandins in the kidney, the main focus of such studies has been on the cardiovascular and insulin functions rather than on the influence of estrogen.

Based on the above experimental data, we found a negative feedback mechanism in the HUK axis. When the ovary cannot secrete estrogen because of functional failure, the brain still orders the reproductive system to secrete hormones, thus causing the abnormal overexpression of estrogen-regulated renal genes, such as Ptgds, which we call a 'fake' response. In theory, Ptgds overexpression will increase the production of downstream metabolites that should have passed through the cell membrane after production, which will then distribute to the corresponding target organs through body fluid circulation. However, we observed an obvious decreasing trend for Ptgds-regulated metabolites in serum and an increasing trend in urine, indicating that these metabolites cannot enter the cardiovascular system through intercellular transfer and that the cell membrane lost its delivery function (Figure 5).

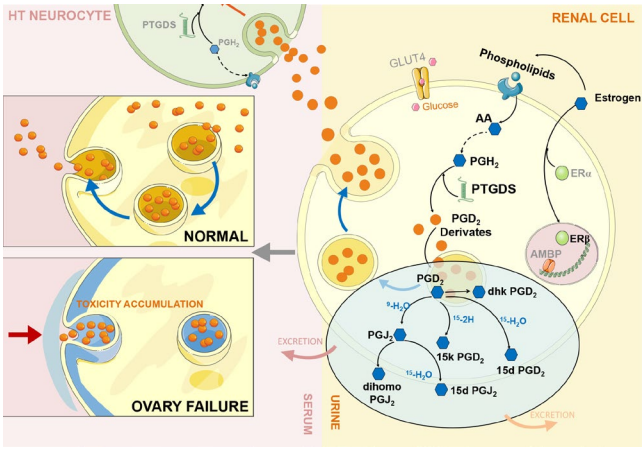

Figure 5. ERβ/Ptgds signalling pathway imbalance disrupting renal lipid metabolism and continues influencing 'hypothalamus-uterus-kidney axis' (HUK axis) function. During ovary failure, a significant downregulation of ERβ (green bubble) leads to PTGDS overexpression (green helix shape) due to persistent releasing 'estrogen secretion' instruction from hypothalamus after ovary failure. We call this 'fake – immunity'. This would further activate the generation of PGD_2 and its derivatives (orange bubbles, each compound represent by blue hexagon shape) in renal cells (yellow cell structure), and inhibit them exert into body fluid circulation through the autocrine and paracrine pathways to reach other intracellular targets (serum: light pink colour; urine: light yellow colour). Therefore, extensively accumulation of these Ptgds regulated metabolites promote kidney lipid toxicity progression (cytoskeleton destruction, grey blue colour part in left panel), then kidney microenvironments disturbance occurs; consequently, inhibition of Ptgds transmission along the 'hypothalamus-uterus-kidney axis' result in its decreased expression in hypothalamus neurocyte (green cell structure). The artwork material from SMART SERVIER MEDICAL ART (Free download, https://smart.servier.com).

We further revealed that estrogen-regulated renal gene overexpression was responsible for the inhibition of the transfer microenvironment, which is an important component of intercellular signalling. Published studies have indicated that the transfer microenvironment refers to a lipid microenvironment composed of membrane-secreting proteins (exosomes), phospholipids, and glycolipids, and its most important function is to facilitate cell signal transduction through corresponding receptors and kinases. In the experiment, we observed a significant decrease in the AA levels in body fluids, indicating that the synthesis of AAs into phospholipids was obstructed, which disturbed the lipid microenvironment. The downstream metabolites of AA were also decreased to balance homeostasis by secreting into specific targets. The perturbation of the lipid microenvironment causes Ptgds-regulated downstream metabolites to excessively accumulate in cells or on cell membranes, which not only produces renal lipid toxicity but also destroys the original transmission function of the cell membrane; therefore, metabolites cannot be transferred between cells, which are why metabolites cannot reach target organs through the circulatory system. More importantly, this finding indicates that Ptgds accumulation in the kidney prevents Ptgds from entering the CNS through an autocrine or bypass secretion pathway where it exerts anti-inflammatory immunity, which may result in degenerative symptoms, such as Alzheimer's disease and sleeping disorders. We confirmed this inference by measuring the reduced Ptgds expression in the hypothalamus and decline spatial learning behaviour.

We found that abnormal GLU, TC, and TG levels were driven by extensive lipid metabolism disorders, such as hyperglycaemia, hyperlipaemia, and abdominal obesity. More importantly, many prostaglandins produced by Ptgds, such as PGD_2 and $15d\text{-}PGJ_2$, were diminished, thus reducing their tumour-inhibiting activity, which may induce breast cancer. Although this pathological phenotype was not observed in this experiment, many published documents have confirmed such mechanisms.

CONCLUSIONS

In conclusion, we present a comprehensive proteomic and metabolomic description of ER-depletion triggered renal function imbalances resulting HUK functions impairment at multiple levels. Our studies found that ERβ-regulated Ptgds overexpression has a significant effect on renal lipid metabolic disorders caused by ovarian failure and further affects brain function. Additional studies are needed to prove whether the dynamic monitoring of abnormal Ptgds expression and the resultant metabolic disorders are reproducible in humans, which may have greater potential for climacteric syndrome predication and therapeutic evaluation as an effective methodological strategy.

MATERIALS AND METHODS

Detailed experimental procedures are provided in Supplementary files.

Chemicals, antibodies, oligonucleotides and reagents

Optima LC grade acetonitrile (ACN) were purchased from Merck, formic acid were purchased from Fluka, water were obtained from Watson. Primary antibodies were purchased from Abcam: ERβ (Abcam, ab3576, RRID: AB_303921), Ptgds (Abcam, ab182141, RRID: AB_2783784),

Animals

SPF female Sprague - Dawley rats (6 - 8 weeks) were obtained from the Fourth Military Medical University Animal Centre. For further details, see Supplementary Experimental Procedures.

Sample preparation

Sample preparation for the urinary proteome

For further details, see Supplementary Experimental Procedures.

Sample preparation for the urinary and serum metabolome

For further details, see Supplementary Experimental Procedures.

Urinary proteome analysis

SDS-PAGE processing

For further details, see Supplementary Experimental Procedures.

iTRAQ labelling and 2D-HPLC-MS/MS analysis

For further details, see Supplementary Experimental Procedures.

Urinary proteomic data processing

For further details, see Supplementary Experimental Procedures.

Gene ontology (GO) annotation and network analyses

For further details, see Supplementary Experimental Procedures.

LC-MS MRM for eicosanoid metabolite determination

For further details, see Supplementary Experimental Procedures.

Metabolite biomarker selection and pathway enrichment

For further details, see Supplementary Experimental Procedures.

Phenotypes evaluation

For further details, see Supplementary Experimental Procedures.

LC-MS scheduled multiple reaction monitoring (MRM) analysis for targeted protein determination

For further details, see Supplementary Experimental Procedures.

Targeted protein confirmation by Immunofluorescence (IF), Western blot (WB), real time PCR and Spatial learning behavior test

For further details, see Supplementary Experimental Procedures.

Statistical analysis

GraphPad Prism 7.0 software (GraphPad Software, La Jolla, CA, USA) was used for the statistical analysis. The statistical analysis for two groups comparisons were conducted using a two-tailed unpaired Student's t-test, for three groups were conducted using one-way ANOVA, followed by Sidak`s multiple comparisons test. Differences with p values < 0.05 were considered significant. No statistical methods were used to predetermine the sample size.

Abbreviations

ER: estrogen receptors; OVX: ovariectomy; IPA: Ingenuity pathway analysis; Ptgds: prostaglandin D2 synthase; HUK axis: hypothalamus-uterus-kidney axis; CKD: chronic kidney disease; E2: oestradiol; IHC: immunohistochemistry; WB: Western blot; qPCR: quantitative PCR; PCA: principal component analysis; PLS-DA: partial least squares-discriminant analysis; AUC: area under the curve; UPLC-TOF/MS: ultra-high-performance liquid chromatography-quadrupole time-of-flight MS; IDA: information-dependent data; Itraq: isobaric tag for relative and absolute quantitation; GO: Gene Ontology; MRM: multiple reaction monitoring; SDS-PAGE: sodium dodecyl sulphate-polyacrylamide gel electrophoresis; KEGG: Kyoto Encyclopedia of Genes and Genomes.

AUTHOR CONTRIBUTIONS

Yan-Ru Liu, Zhi-Shu Tang and Jin-Ao Duan designed the research; Yan-Ru Liu, Zhong-Xing Song, Xin-Yi Kong, Xin-Bo Shi, Yang Lv and Hui-Yuan Zhu performed the research; Yan-Ru Liu, Zhi-Shu Tang, Lin Chen, Rui Zhou and Jing Sun analysed the data; Yan-Ru Liu and Zhi-Shu Tang wrote the paper.

ACKNOWLEDGMENTS

We acknowledge the support of the Shaanxi Province Key Laboratory of New Drugs and Chinese Medicine Foundation Research, Shaanxi Collaborative Innovation Center of Chinese Medicinal Resource Industrialization and KeeCloud Biothech.

CONFLICTS OF INTEREST

The authors declare no conflicts of interest.

FUNDING

This work was supported by the National Natural Science Foundation of China (Project Nos. 81501229, 81904047 and 81773919), The Special Support Program for High-level Personnel Recruitment and the National Youth Talent Support Program supported by Shaanxi Province, The New-Star of Science and Technology supported by Shaanxi Province (2017KJXX-71), Key Research and Development Program of Shaanxi Province (2017SF-364), and The Youth Innovation Team of Shaanxi Universities. Proteomic and metabolomic files: The original proteomic and metabolomic data have been deposited in the figshare database (10.6084/m9.figshare. 7699790, https://figshare.com/s/eed9080292249844e476).

REFERENCES

1. Broekmans FJ, Soules MR, Fauser BC. Ovarian aging: mechanisms and clinical consequences. Endocr Rev. 2009; 30:465–93. https://doi.org/10.1210/er.2009-0006 PMID:19589949

2. Torres MJ, Kew KA, Ryan TE, Pennington ER, Lin CT, Buddo KA, Fix AM, Smith CA, Gilliam LA, Karvinen S, Lowe DA, Spangenburg EE, Zeczycki TN, et al. 17β-Estradiol Directly Lowers Mitochondrial Membrane Microviscosity and Improves Bioenergetic Function in Skeletal Muscle. Cell Metab. 2018; 27:167–179.e7.

https://doi.org/10.1016/j.cmet.2017.10.003 PMID:29103922

3. Vellanki K, Hou S. Menopause in CKD. Am J Kidney Dis. 2018; 71:710–19. https://doi.org/10.1053/j.ajkd.2017.12.019 PMID:29530509

4. Lu R, Kiernan MC, Murray A, Rosner MH, Ronco C. Kidney-brain crosstalk in the acute and chronic setting. Nat Rev Nephrol. 2015; 11:707–19. https://doi.org/10.1038/nrneph.2015.131 PMID:26281892

5. Kurella Tamura M, Yaffe K. Dementia and cognitive impairment in ESRD: diagnostic and therapeutic strategies. Kidney Int. 2011; 79:14–22. https://doi.org/10.1038/ki.2010.336 PMID:20861818

6. Liu YR, Huang RQ, Xiao BK, Yang JY, Dong JX. (1)H NMR metabolic profiling analysis offers evaluation of Nilestriol treatment in ovariectomised rats. Mol Cell Endocrinol. 2014; 387:19–34. https://doi.org/10.1016/j.mce.2014.02.007 PMID:24565896

7. Lumeng CN, Bodzin JL, Saltiel AR. Obesity induces a phenotypic switch in adipose tissue macrophage polarization. J Clin Invest. 2007; 117:175–84. https://doi.org/10.1172/JCI29881 PMID:17200717

8. Readhead B, Haure-Mirande JV, Funk CC, Richards MA, Shannon P, Haroutunian V, Sano M, Liang WS, Beckmann ND, Price ND, Reiman EM, Schadt EE, Ehrlich ME, et al. Multiscale Analysis of Independent Alzheimer's Cohorts Finds Disruption of Molecular, Genetic, and Clinical Networks by Human Herpesvirus. Neuron. 2018; 99:64–82.e7. https://doi.org/10.1016/j.neuron.2018.05.023 PMID:29937276

9. Ge S, Xia X, Ding C, Zhen B, Zhou Q, Feng J, Yuan J, Chen R, Li Y, Ge Z, Ji J, Zhang L, Wang J, et al. A proteomic landscape of diffuse-type gastric cancer. Nat Commun. 2018; 9:1012. https://doi.org/10.1038/s41467-018-03121-2 PMID:29520031

10. Ix JH, Katz R, Bansal N, Foster M, Weiner DE, Tracy R, Jotwani V, Hughes-Austin J, McKay D, Gabbai F, Hsu CY, Bostom A, Levey AS, Shlipak MG. Urine Fibrosis Markers and Risk of Allograft Failure in Kidney Transplant Recipients: A Case-Cohort Ancillary Study of the FAVORIT Trial. Am J Kidney Dis. 2017; 69:410–19. https://doi.org/10.1053/j.ajkd.2016.10.019 PMID:28024930

11. Roberts VS, Cowan PJ, Alexander SI, Robson SC, Dwyer KM. The role of adenosine receptors A2A and A2B signaling in renal fibrosis. Kidney Int. 2014; 86:685–92. https://doi.org/10.1038/ki.2014.244 PMID:25054776

12. Dussol B, Fenouillet E, Brunet P, Purgus R, Sauze N, Carrega L, Mercier L, Zouher I, Bechis G, Berland Y, Guieu R. Kinetic study of adenosine concentrations and the expression of adenosine deaminase in mononuclear cells during hemodialysis. Kidney Int. 2004; 66:1640–46. https://doi.org/10.1111/j.1523-1755.2004.00930.x PMID:15458461

13. Jerebtsova M, Saraf SL, Lin X, Lee G, Adjei EA, Kumari N, Afangbedji N, Raslan R, McLean C, Gordeuk VR, Nekhai S. Identification of ceruloplasmin as a biomarker of chronic kidney disease in urine of sickle cell disease patients by proteomic analysis. Am J Hematol. 2018; 93:E45–47. https://doi.org/10.1002/ajh.24965 PMID:29127684

14. Humphreys BD, Valerius MT, Kobayashi A, Mugford JW, Soeung S, Duffield JS, McMahon AP, Bonventre JV. Intrinsic epithelial cells repair the kidney after injury. Cell Stem Cell. 2008; 2:284–91. https://doi.org/10.1016/j.stem.2008.01.014 PMID:18371453

15. Wei J, Zhang YY, Luo J, Wang JQ, Zhou YX, Miao HH, Shi XJ, Qu YX, Xu J, Li BL, Song BL. The GARP Complex Is Involved in Intracellular Cholesterol Transport via Targeting NPC2 to Lysosomes. Cell Rep. 2017; 19:2823–35. https://doi.org/10.1016/j.celrep.2017.06.012 PMID:28658628

16. Hayek SS, Koh KH, Grams ME, Wei C, Ko YA, Li J, Samelko B, Lee H, Dande RR, Lee HW, Hahm E, Peev V, Tracy M, et al. A tripartite complex of suPAR, APOL1 risk variants and $\alpha_v\beta_3$ integrin on podocytes mediates chronic kidney disease. Nat Med. 2017; 23:945–53. https://doi.org/10.1038/nm.4362 PMID:28650456

17. Chen HH. β-trace protein versus cystatin C: which is a better surrogate marker of renal function versus prognostic indicator in cardiovascular diseases? J Am Coll Cardiol. 2011; 57:859–60. https://doi.org/10.1016/j.jacc.2010.09.052 PMID:21310323

18. Holliday KL, Nicholl BI, Macfarlane GJ, Thomson W, Davies KA, McBeth J. Genetic variation in the hypothalamic-pituitary-adrenal stress axis influences susceptibility to musculoskeletal pain: results from the EPIFUND study. Ann Rheum Dis. 2010; 69:556–60. https://doi.org/10.1136/ard.2009.116137 PMID:19723618

19. Rubinow KB, Henderson CM, Robinson-Cohen C, Himmelfarb J, de Boer IH, Vaisar T, Kestenbaum B, Hoofnagle AN. Kidney function is associated with an altered protein composition of high-density lipoprotein. Kidney Int. 2017; 92:1526–35. https://doi.org/10.1016/j.kint.2017.05.020 PMID:28754556

20. Flyvbjerg A. The role of the complement system in diabetic nephropathy. Nat Rev Nephrol. 2017; 13:311–18. https://doi.org/10.1038/nrneph.2017.31 PMID:28262777

21. Sun J, Furio L, Mecheri R, van der Does AM, Lundeberg E, Saveanu L, Chen Y, van Endert P, Agerberth B, Diana J. Pancreatic β-Cells Limit Autoimmune Diabetes via an Immunoregulatory Antimicrobial Peptide Expressed under the Influence of the Gut Microbiota. Immunity. 2015; 43:304–17. https://doi.org/10.1016/j.immuni.2015.07.013 PMID:26253786

22. Menon MC, Chuang PY, Li Z, Wei C, Zhang W, Luan Y, Yi Z, Xiong H, Woytovich C, Greene I, Overbey J, Rosales I, Bagiella E, et al. Intronic locus determines SHROOM3 expression and potentiates renal allograft fibrosis. J Clin Invest. 2015; 125:208–21. https://doi.org/10.1172/JCI76902 PMID:25437874

23. Ryu S, Chang Y, Kim DI, Kim WS, Suh BS. gamma-Glutamyltransferase as a predictor of chronic kidney disease in nonhypertensive and nondiabetic Korean men. Clin Chem. 2007; 53:71–77. https://doi.org/10.1373/clinchem.2006.078980 PMID:17110470

24. Lu Y, Chen X, Yin Z, Zhu S, Wu D, Chen X. Screening for potential serum biomarkers in rat mesangial proliferative nephritis. Proteomics. 2016; 16:1015–22. https://doi.org/10.1002/pmic.201500405 PMID:26791873

25. Arumugam T, Hwang R, Todd M, Wang H, Brandt W, Westley B, Logsdon C. TFF1 is over expressed early in pancreatic cancer in response to cancer-stromal interactions and stimulates cancer cell invasiveness. Cancer Res. 2007 (9_Supplement); 67:2794. https://cancerres.aacrjournals.org/content/67/9_Supplement/2794

26. Pellefigues C, Dema B, Lamri Y, Saidoune F, Chavarot N, Lohéac C, Pacreau E, Dussiot M, Bidault C, Marquet F, Jablonski M, Chemouny JM, Jouan F, et al. Prostaglandin D_2 amplifies lupus disease through basophil accumulation in lymphoid organs. Nat Commun. 2018; 9:725. https://doi.org/10.1038/s41467-018-03129-8 PMID:29463843

27. Han Z, Zhu T, Liu X, Li C, Yue S, Liu X, Yang L, Yang L, Li L. 15-deoxy-Δ12,14 -prostaglandin J2 reduces recruitment of bone marrow-derived monocyte/macrophages in chronic liver injury in mice. Hepatology. 2012; 56:350–60. https://doi.org/10.1002/hep.25672 PMID:22371273

28. Otsuki M, Gao H, Dahlman-Wright K, Ohlsson C, Eguchi N, Urade Y, Gustafsson JA. Specific regulation of lipocalin-type prostaglandin D synthase in mouse heart by estrogen receptor beta. Mol Endocrinol. 2003; 17:1844–55. https://doi.org/10.1210/me.2003-0016 PMID:12829806

29. Beuckmann CT, Lazarus M, Gerashchenko D, Mizoguchi A, Nomura S, Mohri I, Uesugi A, Kaneko T, Mizuno N, Hayaishi O, Urade Y. Cellular localization of lipocalin-type prostaglandin D synthase (beta-trace) in the central nervous system of the adult rat. J Comp Neurol. 2000; 428:62–78. https://doi.org/10.1002/1096-9861(20001204)428:1<62::AID-CNE6>3.0.CO;2-E PMID:11058225

30. Maesaka JK, Palaia T, Frese L, Fishbane S, Ragolia L. Prostaglandin D(2) synthase induces apoptosis in pig kidney LLC-PK1 cells. Kidney Int. 2001; 60:1692–98. https://doi.org/10.1046/j.1523-1755.2001.00989.x PMID:11703586

31. Fitzpatrick FA, Wynalda MA. Albumin-catalyzed metabolism of prostaglandin D2. Identification of products formed in vitro. J Biol Chem. 1983; 258:11713–18. PMID:6578214

32. Yu J, Kane S, Wu J, Benedettini E, Li D, Reeves C, Innocenti G, Wetzel R, Crosby K, Becker A, Ferrante M, Cheung WC, Hong X, et al. Mutation-specific antibodies for the detection of EGFR mutations in non-small-cell lung cancer. Clin Cancer Res. 2009; 15:3023–28. https://doi.org/10.1158/1078-0432.CCR-08-2739 PMID:19366827

33. Virtue S, Masoodi M, de Weijer BA, van Eijk M, Mok CY, Eiden M, Dale M, Pirraco A, Serlie MJ, Griffin JL, Vidal-Puig A. Prostaglandin profiling reveals a role for haematopoietic prostaglandin D synthase in adipose tissue macrophage polarisation in mice and humans. Int J Obes. 2015; 39:1151–60. https://doi.org/10.1038/ijo.2015.34 PMID:25801691

34. Zhou Y, Shaw N, Li Y, Zhao Y, Zhang R, Liu ZJ. Structure-function analysis of human l-prostaglandin D synthase bound with fatty acid molecules. FASEB J. 2010; 24:4668–77. https://doi.org/10.1096/fj.10-164863 PMID:20667974

35. Nagata N, Fujimori K, Okazaki I, Oda H, Eguchi N, Uehara Y, Urade Y. De novo synthesis, uptake and proteolytic processing of lipocalin-type prostaglandin D synthase, beta-trace, in the kidneys. FEBS J. 2009; 276:7146–58. https://doi.org/10.1111/j.1742-4658.2009.07426.x PMID:19878301

36. Evans JF, Islam S, Urade Y, Eguchi N, Ragolia L. The

lipocalin-type prostaglandin D2 synthase knockout mouse model of insulin resistance and obesity demonstrates early hypothalamic-pituitary-adrenal axis hyperactivity. J Endocrinol. 2013; 216:169–80. https://doi.org/10.1530/JOE-12-0275 PMID:23151358

37. Ragolia L, Palaia T, Hall CE, Maesaka JK, Eguchi N, Urade Y. Accelerated glucose intolerance, nephropathy, and atherosclerosis in prostaglandin D2 synthase knock-out mice. J Biol Chem. 2005; 280:29946–55. https://doi.org/10.1074/jbc.M502927200 PMID:15970590

SUPPLEMENTARY MATERIALS

SUPPLEMENTARY EXPERIMENTAL PROCEDURES

Chemicals, antibodies, oligonucleotides and reagents

Optima LC grade acetonitrile (ACN) were purchased from Merck, formic acid were purchased from Fluka, water were obtained from Watson. Primary antibodies were purchased from Abcam: ERβ (Abcam, ab3576, RRID: AB_303921), Ptgds (Abcam, ab182141, RRID:AB_2783784).

Animals

SPF female Sprague - Dawley rats (6 - 8 weeks) were obtained from the Fourth Military Medical University Animal Centre, maintained in metabolic cages under a 12-h light/dark cycle at 23 ± 2 °C and 55 ± 10% relative humidity and acclimatized for 5 days. Food and drinking water were provided regularly and unrestricted. Body weights were recorded. Rats were ovariectomized at 10 weeks of ages, OVX technical details for all experiments are available in previous study [1, 2]. The rats performed sham surgery was set as control group. For confirmed the targeted proteins, another 3-month Estradiol (E_2) therapy group (OVX+E_2, ig, E2 at 1.5 mg/kg/week) was considered. Animal handling and experimentation were carried in accordance with the guidelines of the Guide for the Care and Use of Laboratory Animals and were approved by the Laboratory Animal Care and Use Committee of the Shaanxi University of Chinese Medicine (Figure 1, Study design).

Sample preparation

Sample preparation for the urinary proteome

For proteomic analysis, 300-μL aliquots of urine were centrifuged twice at 4°C and 10,000×g for 20 min to separate urinary proteins from small molecules using an Amicon Ultra 0.5-mL Centrifugal Filter (10 kDa, UFC501096, Merck Millipore, Germany) according to the manufacturer's instructions. The proteins captured in the filter were washed with water three times at 4°C and 10,000×g for 30 min to remove possible interferences. Then, the concentrated ultrafiltrate was centrifuged at 3,000×g for 1 min and freeze-dried for protein determination. All urinary solutions were stored at -20°C until use.

Sample preparation for the urinary and serum metabolome

For metabolomic analysis, primary urinary and serum samples were prepared according published procedures [1].

Urinary proteome analysis

SDS-PAGE processing

The total protein concentration was measured in each sample using a BCA Protein Assay Kit (Thermo Scientific, Waltham, MA, USA) at an absorbance of 570 nm, referenced by standard curve. Urinary proteins were fractionated by sodium dodecyl sulfate - polyacrylamide gel electrophoresis (SDS - PAGE).

iTRAQ labelling and 2D-HPLC-MS/MS analysis

Each 200-μg extract sample was prepared following standard digestion, reduction, and alkylation procedures prior to isobaric tag for relative and absolute quantitation (iTRAQ) labelling [3]. Peptide labelling (114-117) with iTRAQ reagent was performed following the manufacturer's protocol. The four isotopic iTRAQ labelling samples were combined and were fractionated on a waters UPLC using a C18 column (waters BEH C18 2.1 ×50mm, 1.7um). Peptides were eluted at a flow rate of 600Ml / min with a linear gradient of 5~35% solvent B (acetonitrile) over 10 min, the solvent A is 20mM ammonium formate with pH adjusted to 10. The absorbance at 214 nm was monitored, and a total of 10 fractions were collected. The fraction was separated by nano-HPLC (Eksigent Technologies) on the secondary RP analytical column (Eksigent, C18, 3μm, 150 mm ×75μm), using a gradient mobile phase 98% acetonitrile - 2% milli Q water (A) and 0.1% formic acid (B), at a flow rate of 0.3 μL / min, the gradient program was as follows: 0-5 min: 5% B, 6-65 min: 5-40% B, 65-66 min: 40-80% B, 66-71 min: 80% B, 71-72 min: 80-5% B, and 72-90 min: 5% B. Full scan and tandem mass spectrometry experiments were duplicated again on an AB SCIEX TripleTOF 5600 system. Information-dependent data (IDA) acquisition mode was used to switch automatically between MS and MS/MS acquisition with the following parameters: an ion spray voltage of 2,500 V, curtain gas (CUR) of 25 p.s.i., a cycle time of 1 s, and a dwell time of 30 ms. MS spectra were acquired between 350~1250 m/z (molecular weight/valency) in high-resolution mode (40,000 resolution for full scans and 20,000 resolution for MS/MS scans) with rolling collision energy on via 250-ms accumulation time/spectrum and 50-mDa mass tolerance, and the 10 most intense precursors per cycle were selected for fragmentation with a dynamic exclusion time of 30 s. Data acquisition was conducted using Analyst 2.0 software (AB SCIEX).The collected samples were re-suspended in in 0.1% formic acid solution (0.1% formic acid - 2%

acetonitrile - 98% milli Q water) and analysed on a Eksigent C18 column (150 mm × 75 µm, 3 µm), using a gradient mobile phase 98% acetonitrile-2% milli Q water (A) and 0.1% formic acid (B), at a flow rate of 0.3 µL/min, the gradient program was as follows: 0-5 min: 5% B, 6-65 min: 5-40% B, 65-66 min: 40-80% B, 66-71 min: 80% B, 71-72 min: 80-5% B, and 72-90 min: 5% B.

Urinary proteomic data processing

Original data (*.wiff, *.wiff.scan) acquired from the MS/MS analysis in each LC run were converted to Mascot generic files (*.mgf) using ProteinPilot 4.5 software (AB SCIEX). The MS/MS peak lists of the formatted data were then searched by Mascot (Matrix Science, London, UK; version 2.3.02), spectra were searched against the UniProt database, and the taxonomy was set to Rat. Scaffold (version Scaffold_4.4.5, Proteome Software Inc., Portland, OR) was used to validate MS/MS based peptide and protein identifications.

Gene ontology (GO) annotation and network analyses

Protein annotation was subject to GO analysis on the basis of biological responses or disease analysis for biological processes, molecular functions, and cellular components. The differentially expressed proteome (> 1.5-fold changes in all ratios) from the iTRAQ LC-MS/MS analysis of urinary samples was interpreted using Ingenuity Pathway Analysis 9.1 (Ingenuity Systems, Mountain View, CA, USA, www.ingenuity.com) [4]. To conduct a pathway analysis and identify proteins connected to pathways of interest, both upregulated and downregulated proteins were computed in accordance with each network [5, 6].

We additionally used the hypothesis strategy GeneMANIA (application version 3.6.0, *Rattus norvegicus*, freely available at http://genemania.org) to generate hypotheses regarding gene function and calculate gene lists and weighting genes, the algorithm of which is designed to automatically weight networks on the basis of levance to the gene set. To evaluate the significance of selected proteins from the observed network, we performed multiple gene queries to identify the most closely connected genes among the networks and attributes selected from IPA enrichment. Physical interactions, pathways, and genetic interactions were generated, and the datasets relevant to ovarian failure and the pro-survival signalling network were collected [7–9].

LC-MS MRM for eicosanoid metabolite determination

The LC-MS semi-quantification analysis of eicosanoids was conducted on the AB QTrap 4500 - Agilent 1260 LC-ESI/MS system (AB SCIEX, Agilent Technologies). A 5-µL aliquot of each urine sample was injected onto an Agilent ZORBAX Eclipse Plus C_{18} column (100 mm × 4.6 mm, 5 µm; Agilent Technologies) with a mobile phase consisting of 0.1% formic acid in water (A) and 0.1% formic acid in acetonitrile (B). Gradient elution was carried out for 35 min at a flow rate of 0.8 mL/min, and the optimized gradient process was set as follows: 0-25 min: 0.2% -100% B, 25-30 min: 100% B, 30-31 min: 100%-0.2% B, and 31-35 min: 0.2% B. The column temperature was maintained at 30°C. Quantified MS data were obtained with an electrospray ionization (ESI) source in negative ion (NI, 4.5 kV) mode under the following conditions: CUR, 25 p.s.i.; temperatures, 450°C; gas source 1 and gas source 2, 40°C, respectively, referring to the method published by Yan Wang *et al.* [10]. All data were obtained using Analyst 1.6.2 software (Applied Biosystems), and the metabolites were quantified using Multiquant software (Applied Biosystems) (Supplementary Figure 1, and Supplementary Table 1).

Metabolite biomarker selection and pathway enrichment

To identify biomarkers and construct a metabolite set, a multivariate statistical analysis, including principal component analysis (PCA), partial least squares-discriminant analysis (PLS-DA), t-tests, and area under the curve (AUC) analysis, was applied using the MetaboAnalyst 4.0 online platform (available online at http://www.metaboanalyst.ca) [11]. For more consistent and robust biomarker selection and to reduce study biases to facilitate more robust biomarker identification across different experiments on ovarian failure, three batches of data with a sample size capacity of 85 were conducted using the biomarker 'meta-analysis' process on MetaboAnalyst 4.0 [12]. To reveal important links among 'genes, metabolites, and diseases', we next selected the network explorer using the SIMCA-P software (14.1 version) module to represent a comprehensive knowledge base of 'renal lipid metabolism disorder-genes-metabolites' induced by ovarian failure for interactive network visualization [13].

Phenotypes evaluation

Body weight was monitored weekly, while the organ to body weight ratio (including the liver, kidneys, spleen, uterus, cerebrum, and hypothalamus) were determined at 12 week of the experiment. Biochemical assays were evaluated 12 weeks after rats were OVX. Complete histopathology assays from organs were also performed.

LC-MS scheduled multiple reaction monitoring (MRM) analysis for targeted protein determination

To understand the underlying ovarian failure-driven transformation process in the 'hypothalamus-uterus-kidney axis', we performed MRM-based targeted

proteomics. Briefly, a representative peptide was chosedchosen for one targeted protein. Heavy isotope-labeled peptides were ordered from BANKPEPTIDE LTD (Hefei China). Each sample was spiked in heavy isotope-labeled peptide. (the detailed optimization information for each protein is listed in Supplementary Table 2) [16, 17]. MRM experiments were performed on a 6500 QTRAP hybrid triple quadrupole/linear ion trap mass spectrometer (AB Sciex, Foster City, CA) interfaced with an Eksigent nano 1D plus system (Waters, Milford, MA). MRM transitions were monitored using unit resolution in both Q1 and Q3 quadrupoles to maximize specificity. Data analyses were performed using SKYLINE (version 2.6).

Targeted protein confirmation by Immunofluorescence (IF), Western blot (WB), real time PCR and Spatial learning behavior test

IF

For double staining with uterus, hypothalamus, and kidney tissues, primary antibody for ERβ (Abcam, ab3576, 1:100), or PTGDS (Abcam, ab182141, 1:3000) was incubated overnight at 4 ºC . After the primary antibodies had been applied, the sections were sequentially incubated with HRP-conjugated secondary antibody (goat anti-rabbit IgG, ab6721, abcam) and CY3-conjugated secondary antibody (goat anti-rabbit IgG, ab6939, abcam). 4',6-diamidino-2-phenylindole (DAPI) was used for nuclear staining. The sections were observed under an upright fluorescence microscope (NIKON ECLIPSE C1, Nikon, Japan) connected to a scanning system (NIKON DS-U3, Nikon, Japan) coupled with the digital slide viewer NDP.scan (version 3.2.12, Hamamatsu Photonics, Shizuoka Pref., Japan). Image-Pro plus 6.0 software was used to measure the staining area to obtain the integrated optical density (IOD) and staining area (AREA) values. Then the AOD ratio indicates the ratio of IOD to AREA, that a larger AOD ratio represents a higher protein expression level.

WB

We next confirmed whether the selected anormaly expressed proteins had effect on 'hypothalamus-uterus-kidney' axis. The hypothalamus, uterus, and kidneys tissues were removed from control and OVX rats and subjected to western blot analysis. The proteins were transferred onto nitrocellulose membranes. After blocking in 5% BSA-TBST (Sigma), the membranes were incubated with the following primary antibodies from Abcam at 4°C overnight: ERβ (1:1000, ab3576), and Ptgds (1:1000, ab182141). Blots were then washed and incubated with the appropriate secondary antibody for 40 min at room temperature. Blot bands were visualized using chemiluminescence (ECL, WBKLS0500, Millipore). Relative band pixel intensities were semi-quantified using ImageJ software (NIH), and protein loading was normalized using an antibody against β-actin (A5441; Sigma-Aldrich) [15].

Real time PCR

100 mg of uterus, hypothalamus, and renal kidney were homogenized in TRIzol reagent (Servicebio) to extract total RNA, and 1 mg RNA was reverse-transcribed using RevertAid First Strand cDNA Synthesis Kit (#K1622, Thermo). Quantitative PCR was performed in a ViiaTM 7 Real-Time PCR System (Life Technologies, Grand Island, NY) using FastStart Universal SYBR Green Master (Rox) reagent (04 913 914 001, Roche). Assays were performed in triplicates and final values were normalized to ribosomal Ptgds or ERβ mRNA levels. The oligonucleotides (Invitrogen) for PCR as follows: rat Ptgds (ref. NM_013015.2, 296 bp, 60°C, Servicebio): forward primer: 5′- CAGCCCAACTTTCAACAAGACA -3′ and reverse primer: 5′- GCGTACTCATCGTAGTCG GTTTC -3′; rat ERβ (ref. NM_012754.1, 204 bp, 60°C, Servicebio): forward primer: 5`- CTGGGTGATTGCGA AGAGTGG -3′ and reverse primer: 5′- GAGGACTTGT ACCCTCGAAGCG -3′.

Spatial learning behavior test (Morris water maze test)

All behavioral testing protocols were approved by the Laboratory Animal Care and Use Committee of the Shaanxi University of Chinese Medicine. The Morris water maze (MWM) test for rats` location and spatial learning was conduct in a 130 cm diameter white plastic maze (130cm diameter ×50cm height) and surrounded by opacity curtains from 9:00–11:00 AM. The maze was filled with opaque water (Titanium powder dyed white, 20~22^{o} C) and contained a goal (PVC circular escape platform: 10 cm diameter × 22cm height) submerged 1cm below the water surface to keep the rats out of sight.

Location test: After 5 days pretraining procedures, each rat (the head top was dyed in yellow colour) was placed into the water facing the wall on the randomized quadrant points, the timing is stared the moment that the rat is released. When the rat touched the platform and stayed for at least 3s, timing is stopped. Once the rats located the platform, it was allowed to stay for 10 s. Rats not finding the platform within 90s limit are either placed on the platform or guided to it. During each trial, the data of escape latency and swim length were monitored automatically from the digitized image *via* image tracking system (WMT-100S, Chengdu Technology & Market Corp., LTD, China).

Spatial learning test: The spatial learning test was conducted on continuous training day 6 after location test. The invisible platform was removed and the rat was released at a new start position and repeat the trial. During each trial, the data of total number of platform site crossings was monitored.

Statistical analysis

GraphPad Prism 7.0 software (GraphPad Software, La Jolla, CA, USA) was used for the statistical analysis. The statistical analysis for two groups comparisons were conducted using a two-tailed unpaired Student's t-test, for three groups were conducted using one-way ANOVA, followed by Sidak`s multiple comparisons test Differences with p values < 0.05 were considered significant. No statistical methods were used to predetermine the sample size.

REFERENCES

1. Liu YR, Huang RQ, Xiao BK, Yang JY, Dong JX. (1)H NMR metabolic profiling analysis offers evaluation of Nilestriol treatment in ovariectomised rats. Mol Cell Endocrinol. 2014; 387:19–34. https://doi.org/10.1016/j.mce.2014.02.007 PMID:24565896

2. Liu YR, Xiao BK, Yang JY, Guo CH, Shen SJ, Tang ZS, Dong JX, Huang RQ. 1 H-NMR and HPLC–MS/MS-based global/targeted metabolomic evaluation of Hypericum perforatum L. intervention for menopause. J Funct Foods. 2015; 17:722–41. https://doi.org/10.1016/j.jff.2015.06.023

3. Shevchenko A, Tomas H, Havlis J, Olsen JV, Mann M. In-gel digestion for mass spectrometric characterization of proteins and proteomes. Nat Protoc. 2006; 1:2856–60. https://doi.org/10.1038/nprot.2006.468 PMID:17406544

4. Ix JH, Katz R, Bansal N, Foster M, Weiner DE, Tracy R, Jotwani V, Hughes-Austin J, McKay D, Gabbai F, Hsu CY, Bostom A, Levey AS, Shlipak MG. Urine Fibrosis Markers and Risk of Allograft Failure in Kidney Transplant Recipients: A Case-Cohort Ancillary Study of the FAVORIT Trial. Am J Kidney Dis. 2017; 69:410–19. https://doi.org/10.1053/j.ajkd.2016.10.019 PMID:28024930

5. Ashburner M, Ball CA, Blake JA, Botstein D, Butler H, Cherry JM, Davis AP, Dolinski K, Dwight SS, Eppig JT, Harris MA, Hill DP, Issel-Tarver L, et al, and The Gene Ontology Consortium. Gene ontology: tool for the unification of biology. Nat Genet. 2000; 25:25–29. https://doi.org/10.1038/75556 PMID:10802651

6. Harris MA, Clark J, Ireland A, Lomax J, Ashburner M, Foulger R, Eilbeck K, Lewis S, Marshall B, Mungall C, Richter J, Rubin GM, Blake JA, et al, and Gene Ontology Consortium. The Gene Ontology (GO) database and informatics resource. Nucleic Acids Res. 2004; 32:D258–61. https://doi.org/10.1093/nar/gkh036 PMID:14681407

7. Franz M, Rodriguez H, Lopes C, Zuberi K, Montojo J, Bader GD, Morris Q. GeneMANIA update 2018. Nucleic Acids Res. 2018; 46:W60–W64. https://doi.org/10.1093/nar/gky311 PMID:29912392

8. Vlasblom J, Zuberi K, Rodriguez H, Arnold R, Gagarinova A, Deineko V, Kumar A, Leung E, Rizzolo K, Samanfar B, Chang L, Phanse S, Golshani A, et al. Novel function discovery with GeneMANIA: a new integrated resource for gene function prediction in Escherichia coli. Bioinformatics. 2015; 31:306–10. https://doi.org/10.1093/bioinformatics/btu671 PMID:25316676

9. Pirooznia M, Wang T, Avramopoulos D, Potash JB, Zandi PP, Goes FS. High-throughput sequencing of the synaptome in major depressive disorder. Mol Psychiatry. 2016; 21:650–55. https://doi.org/10.1038/mp.2015.98 PMID:26216301

10. Wang Y, Armando AM, Quehenberger O, Yan C, Dennis EA. Comprehensive ultra-performance liquid chromatographic separation and mass spectrometric analysis of eicosanoid metabolites in human samples. J Chromatogr A. 2014; 1359:60–69. https://doi.org/10.1016/j.chroma.2014.07.006 PMID:25074422

11. Xia J, Psychogios N, Young N, Wishart DS. MetaboAnalyst: a web server for metabolomic data analysis and interpretation. Nucleic Acids Res. 2009; 37:W652–60. https://doi.org/10.1093/nar/gkp356 PMID:19429898

12. Chong J, Soufan O, Li C, Caraus I, Li S, Bourque G, Wishart DS, Xia J. MetaboAnalyst 4.0: towards more transparent and integrative metabolomics analysis. Nucleic Acids Res. 2018; 46:W486–94. https://doi.org/10.1093/nar/gky310 PMID:29762782

13. Xia J, Gill EE, Hancock RE. NetworkAnalyst for statistical, visual and network-based meta-analysis of gene expression data. Nat Protoc. 2015; 10:823–44. https://doi.org/10.1038/nprot.2015.052 PMID:25950236

14. Yu J, Kane S, Wu J, Benedettini E, Li D, Reeves C, Innocenti G, Wetzel R, Crosby K, Becker A, Ferrante M, Cheung WC, Hong X, et al. Mutation-specific antibodies for the detection of EGFR mutations in non-small-cell lung cancer. Clin Cancer Res. 2009; 15:3023–3028.

https://doi.org/10.1158/1078-0432.CCR-08-2739 PMID:19366827

15. Mao K, Quipildor GF, Tabrizian T, Novaj A, Guan F, Walters RO, Delahaye F, Hubbard GB, Ikeno Y, Ejima K, Li P, Allison DB, Salimi-Moosavi H, et al. Late-life targeting of the IGF-1 receptor improves healthspan and lifespan in female mice. Nat Commun. 2018; 9:2394. https://doi.org/10.1038/s41467-018-04805-5 PMID:29921922

16. Chen C, Liu X, Zheng W, Zhang L, Yao J, Yang P. Screening of missing proteins in the human liver proteome by improved MRM-approach-based targeted proteomics. J Proteome Res. 2014; 13: 1969–78. https://doi.org/10.1021/pr4010986 PMID:24597967

17. Kim Y, Jeon J, Mejia S, Yao CQ, Ignatchenko V, Nyalwidhe JO, Gramolini AO, Lance RS, Troyer DA, Drake RR, Boutros PC, Semmes OJ, Kislinger T. Targeted proteomics identifies liquid-biopsy signatures for extracapsular prostate cancer. Nat Commun. 2016; 7:11906. https://doi.org/10.1038/ncomms11906 PMID:27350604

Supplementary Figures

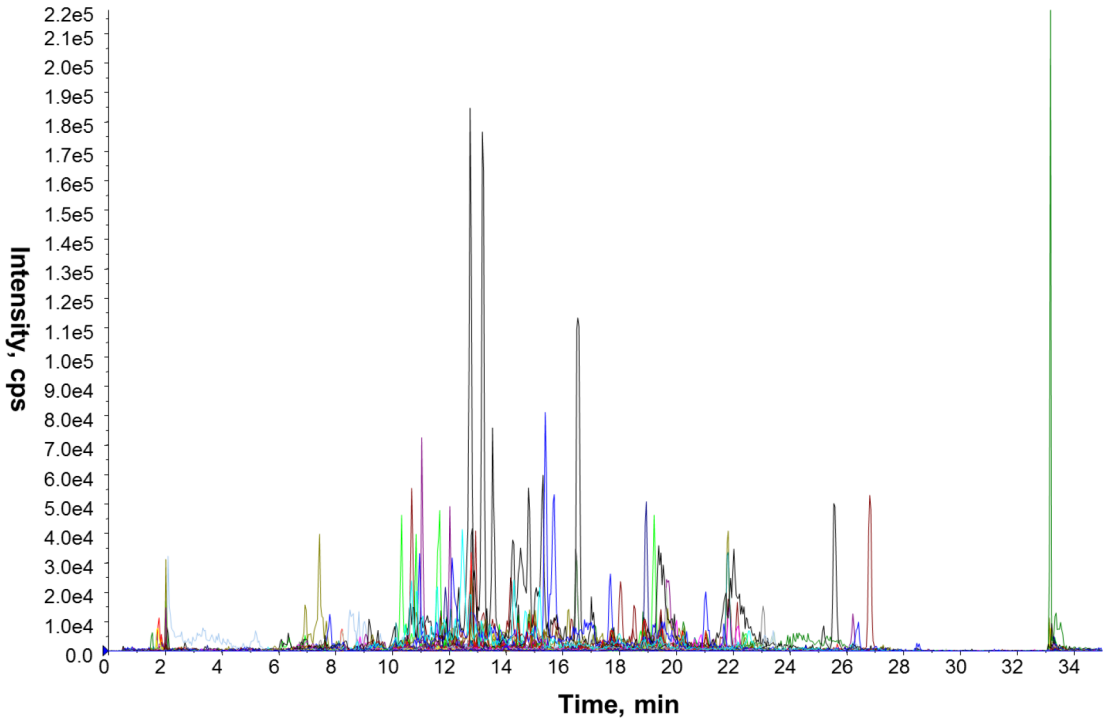

Supplementary Figure 1. Representative HPLC-ESI/MS MRM total ion chromatograms (TIC) of 155 eicosanoids.

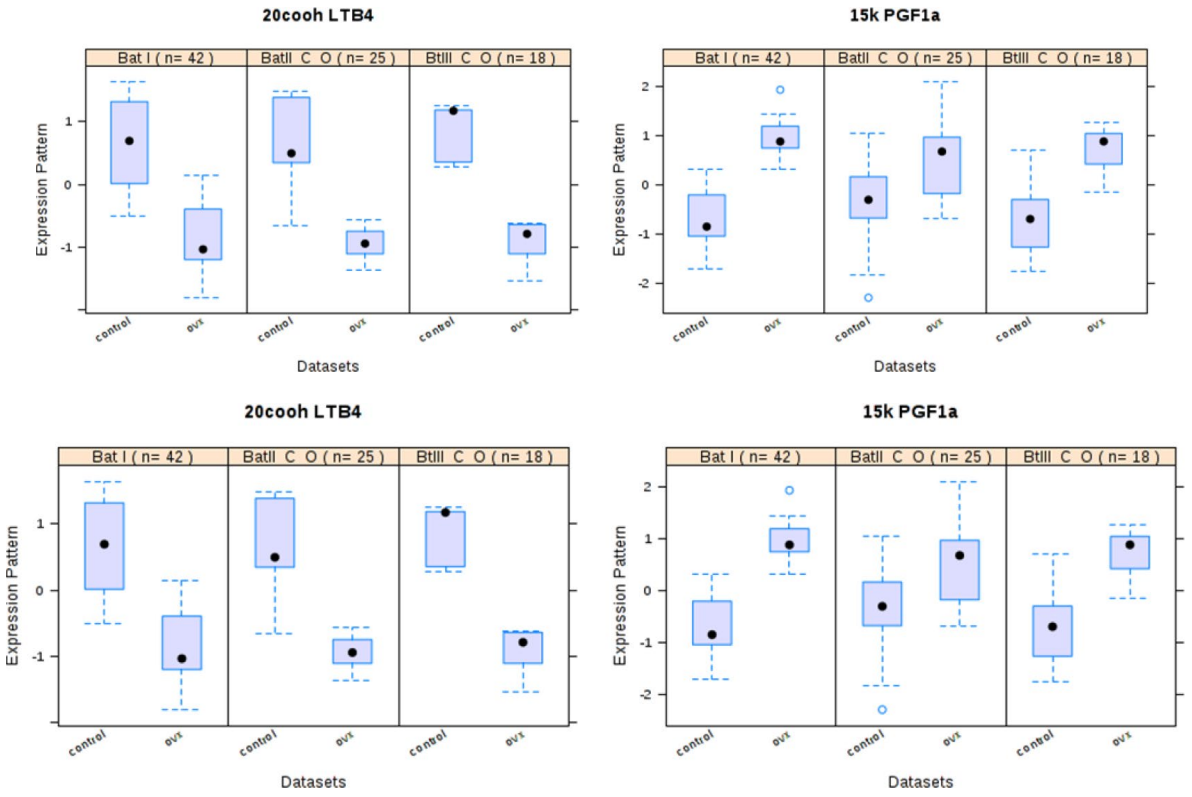

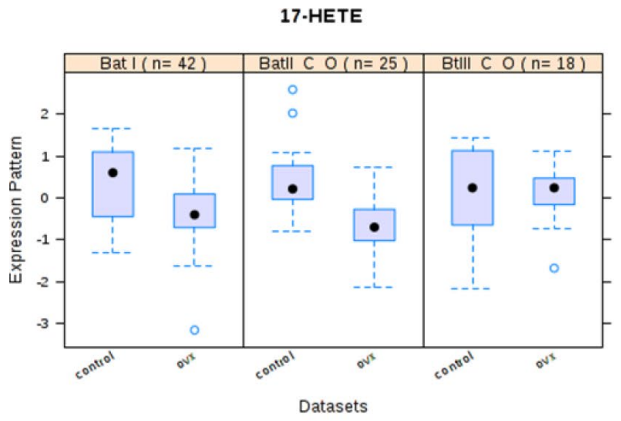
17-HETE
Bat I (n= 42)
BatII C O (n= 25)
BtIII C O (n= 18)
Expression Pattern
control
ovs
Datasets

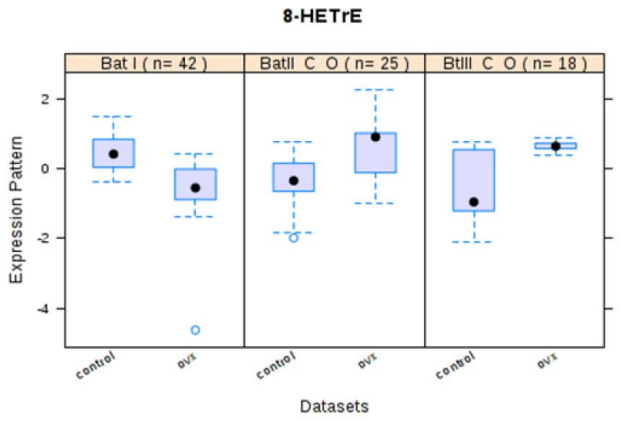
8-HETrE
Bat I (n= 42)
BatII C O (n= 25)
BtIII C O (n= 18)
Expression Pattern
control
ovs
Datasets

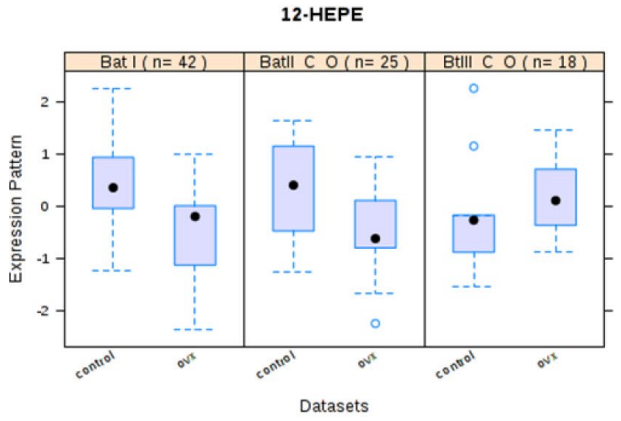
12-HEPE
Bat I (n= 42)
BatII C O (n= 25)
BtIII C O (n= 18)
Expression Pattern
control
ovs
Datasets

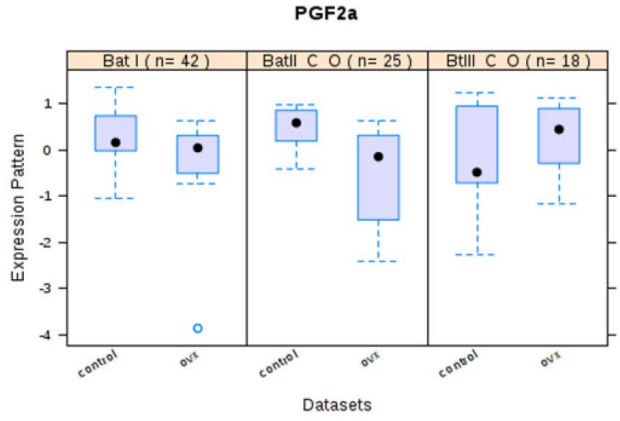
PGF2a
Bat I (n= 42)
BatII C O (n= 25)
BtIII C O (n= 18)
Expression Pattern
control
ovs
Datasets

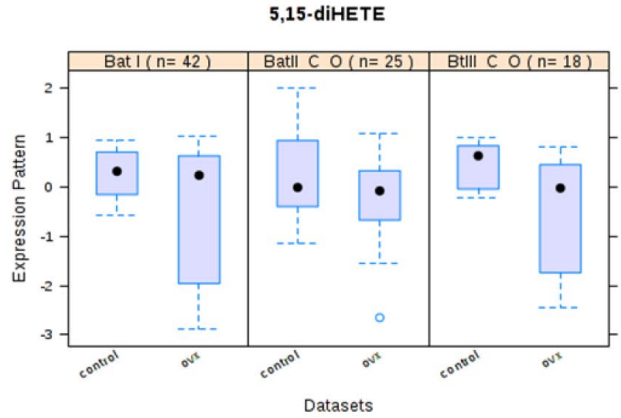
5,15-diHETE
Bat I (n= 42)
BatII C O (n= 25)
BtIII C O (n= 18)
Expression Pattern
control
ovs
Datasets

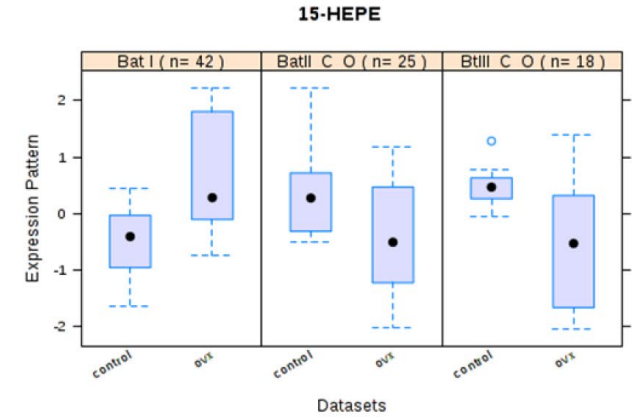
15-HEPE
Bat I (n= 42)
BatII C O (n= 25)
BtIII C O (n= 18)
Expression Pattern
control
ovs
Datasets

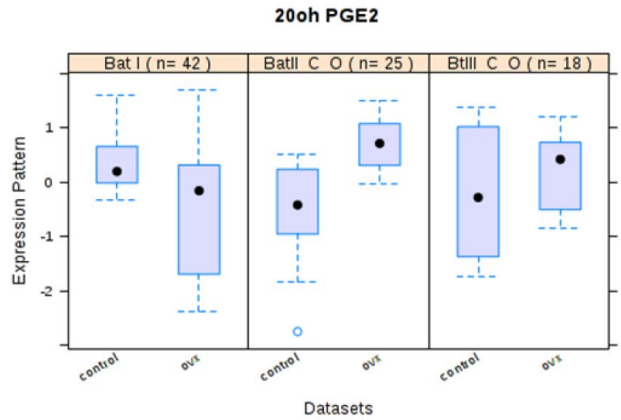
20oh PGE2
Bat I (n= 42)
BatII C O (n= 25)
BtIII C O (n= 18)
Expression Pattern
control
ovs
Datasets

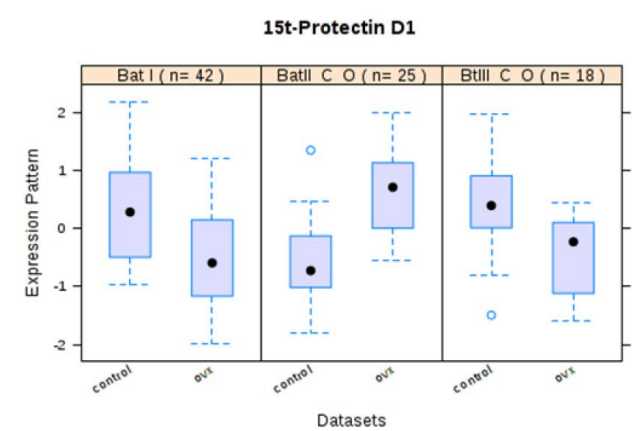
15t-Protectin D1
Bat I (n= 42)
BatII C O (n= 25)
BtIII C O (n= 18)
Expression Pattern
control
ovs
Datasets

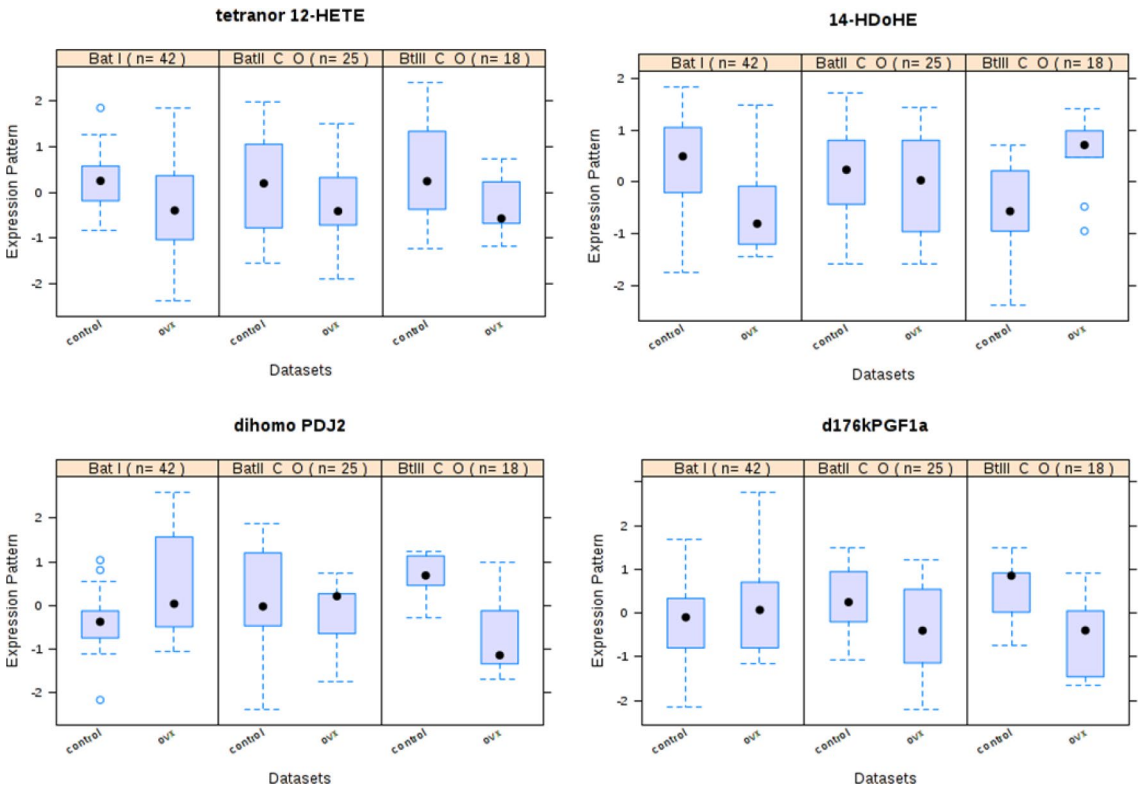

Supplementary Figure 2. Box plot of the expression pattern of the selected feature between the two experimental groups across all studies. The expression pattern is on the y-axis, and the group labels are on the x-axis. The median expression for the feature is indicated with a black dot in the center of the boxplot.

Supplementary Tables

Please browse Full Text version to see the data of Supplementary Table 1.

Supplementary Table I. Optimized MRM pairs of LC/MS–MS for the 155 eicosanoids.

Supplementary Table 2. Targeted proteins MRM for Q1>Q3, DP, CE Optimization.

Protein	Peptide	Q1*	Q3*	DP	CE	ion type	Lable**
Prostaglandin-H2 D-isomerase	DQGLTEEDIVFLPQPDK	648.658072	844.4563	78.4	32.9	+3y7	light
		648.6581	697.3879	78.4	32.9	+3y6	light
		648.6581	584.3039	78.4	32.9	+3y5	light
		648.6581	301.1143	78.4	32.9	+3b3	light
		651.3295	852.4705	78.4	32.9	+3y7	heavy
		651.3295	705.4021	78.4	32.9	+3y6	heavy
		651.3295	592.3181	78.4	32.9	+3y5	heavy
		651.3295	301.1143	78.4	32.9	+3b3	heavy

*Q1 is the peptide precursor ion, and Q3 is the peptide product ion, DP is the declustering potential, and CE is the collision energy.
**Light: target peptide; Heavy: standards.

Please browse Full Text version to see the data of Supplementary Table 3.

Supplementary Table 3. Enrichment list of differentially expressed proteins on cellular component, cellular function, and biochemical process. (cut-off valure 1.5-fold change, p value < 0.05).

Supplementary Table 4. Top 5 disease and disorders predicted by IPA.

Disease	p-value	Molecules count	Molecules
Neurological Disease	3.61E-09-4.26E-03	22	DPP4,PVALB,C3,ACTB,CP,SOD1,PTGDS,GSN,LIFR,HSPA8,COL1A1,CDH1,CTSA,MYH2,ATP5B,GAA,ANXA1,EIF4A1,MYH3,PSAP,AFM,PLAU
Reproductive System Disease	1.23E-04-2.98E-03	20	DPP4,SERPINA6,MYH6,C3,LPO,CP,KRT5,PTGDS,SOD1,GSN,LIFR,COL1A1,CDH1,CAMP,WFDC2,ANXA1,EIF4A1,SLC3A1,AFM,PLAU
Metabolic Disease	1.52E-04-4.26E-03	17	DPP4,C3,ACTB,CP,PTGDS,SOD1,GSN,HSPA1L,COL1A1,Glycam1,CTSA,ANXA1,GAA,PSAP,AFM,PLAU,NPC2
Renal and Urological System Development and Function	1.56E-04-1.86E-03	4	CDH1,CAMP,C3,PLAU
Renal and Urological Disease	4.59E-04-2.13E-03	5	PVALB,DPP4,C3,PSAP,PTGDS

Supplementary Table 5. Top toxicity functions predicted by IPA.

Name	p-value	Overlap (select/identify)
Acute Renal Failure Panel (Rat)	9.18E-06	6.5 % (4/62)
Long-term Renal Injury Anti-oxidative Response Panel (Rat)	6.66E-04	11.1 % (2/18)
Positive Acute Phase Response Proteins	1.86E-03	6.7 % (2/30)
Persistent Renal Ischemia-Reperfusion Injury (Mouse)	1.86E-03	6.7 % (2/30)

Supplementary Table 6. Top 5 molecular and cellular functions predicted by IPA.

Name	p-value	Molecules count	Molecules
Cell Morphology	8.51E-08-3.31E-03	20	PVALB,DPP4,MYH6,C3,ACTB,AMBP,CP,PTGDS,SOD1,GSN,COL1A1,CTSA,CDH1,CAMP,MYH2,GAA,ANXA1,PSAP,PLAU,Tpm3
Tissue Morphology	8.51E-08-2.98E-03	18	MYH6,C3,AMBP,CP,PTGDS,SOD1,GSN,LIFR,COL1A1,CDH1,MYH2,CAMP,GAA,ANXA1,PSAP,PLAU,Tpm3,NPC2
Lipid Metabolism	4.41E-06-4.09E-03	15	DPP4,SERPINA6,PVALB,C3,CP,PTGDS,SOD1,GSN,HSPA1L,HSPA8,CAMP,ANXA1,PSAP,PLAU,NPC2
Cell-To-Cell Signaling and Interaction	5.27E-06-3.46E-03	16	DPP4,C3,ACTB,CD300LD,CP,SOD1,GSN,HSPA1L,LIFR,HSPA8,Glycam1,CDH1,CAMP,ANXA1,PSAP,PLAU
Cellular Function and Maintenance	5.27E-06-4.2E-03	17	S100vp,C3,ACTB,CP,SOD1,PTGDS,GSN,HSPA1L,HSPA8,COL1A1,CDH1,MYH2,CAMP,ANXA1,GAA,PSAP,PLAU

Supplementary Table 7. Top 5 associated network predicted by IPA.

ID	Top diseases and functions	Score	Focus molecules	Molecules in network
1	Cellular Movement, Hematological System Development and Function, Immune Cell Trafficking	42	18	AMBP, ANXA1, C3, CAMP, CDH1, COL1A1, Collagen type I, Collagen(s), CP, DPP4, elastase, ERK1/2, Fibrin, Fibrinogen, Growth hormone, GSN, HDL, IL12 (complex), Integrin, LDL, LIFR, LOC299282, LPO, Mmp, NPC2, PLAU, Pld, Pro-inflammatory Cytokine, Prss1 (includes others), PTGDS, Secretase gamma, SERPINA6, STAT5a/b, trypsin, WFDC2
2	Cellular Growth and Proliferation, Hematopoiesis, Cell Death and Survival	30	14	AMBP, AR, C2, CHUK, CNN3, Cpla2, CTSA, FAS, FNDC5, Glycam1, GSN, HNF4A, HPGDS, ITIH3, K Channel, LIFR, MAPK14, MYH2, MYOD1, PNAD, PODXL, PTGDS, PVALB, Pzp, RPS27A, Scgb1b27 (includes others), Scgb2b27 (includes others), SCPEP1, SUSD2, TGFB1, TNFAIP2, TP53, Tpm3, Tpm4, WISP3
3	Cell-To-Cell Signaling and Interaction, Carbohydrate Metabolism, Lipid Metabolism	11	7	AMBP,CALB1,CAMP,CD55,CD300LD,CLCF1,Cpla2,CXCR2,ERK,estrogen receptor, Focal adhesion kinase, FSH, IL36B, IL36G, Insulin, Jnk, JUN/JUNB/JUND, K Channel, Kng1/Kng1l1, LBP, LOC500183, Mac, Mapk, miR-146a-5p, MUC2, NFkB (complex), NFKBIA, P2RX7, P38 MAPK, p85 (pik3r), Pkc(s), PLA2G6, PLC, PTGDS, SLC3A1, Vegf

Supplementary Table 8. Top analysis-ready molecules predicted by IPA (FC).

GeneName	Abbreviations	FC	p value
Protein AMBP	Ambp↑	1.787	2.415E-07
Prostaglandin-H2 D-isomerase	Ptgds↑	1.521	1.591E-05
Annexin A1	Anxa1↓	0.601	9.868E-05
Complement C3	C3↓	0.568	4.663E-05
Cathelicidin antimicrobial peptide	Camp↓	0.377	5.069E-04
Collagen alpha-1(I) chain	Col1a1↓	0.562	9.670E-06
Leukemia inhibitory factor receptor	Lifr↓	0.651	9.233E-06
Myosin-6	Myh6↓	0.613	4.583E-04

Symbol	Score	Functions	Links
Camp	0.947235	disruption of cells of other organism, disruption of cells of other organism involved in symbiotic interaction, killing of cells in other organism involved in symbiotic interaction, killing of cells of other organism	http://www.ncbi.nlm.nih.gov/sites/entrez?db=gene&cmd=search&term=316010
Myh6	0.677982	blood circulation, structural molecule activity	http://www.ncbi.nlm.nih.gov/sites/entrez?db=gene&cmd=search&term=29556
Esr2	0.665631	response to estradiol, response to estrogen, vagina development	http://www.ncbi.nlm.nih.gov/sites/entrez?db=gene&cmd=search&term=25149
Lifr	0.649731	growth factor binding, muscle cell apoptotic process, negative regulation of muscle cell apoptotic process, organ regeneration, regeneration, regulation of muscle cell apoptotic process	http://www.ncbi.nlm.nih.gov/sites/entrez?db=gene&cmd=search&term=81680
Col1a1	0.597373	cellular response to acid, cellular response to amino acid stimulus, collagen, collagen fibril organization, extracellular matrix, extracellular matrix organization, extracellular matrix part, extracellular matrix structural constituent, extracellular structure organization, fibrillar collagen, growth factor binding, platelet-derived growth factor binding, protein heterotrimerization, proteinaceous extracellular matrix, response to amino acid, response to corticosteroid, response to estradiol, response to estrogen, skin development, structural molecule activity, wound healing	http://www.ncbi.nlm.nih.gov/sites/entrez?db=gene&cmd=search&term=29393
Ptgds	0.577912	response to corticosteroid, response to glucocorticoid	http://www.ncbi.nlm.nih.gov/sites/entrez?db=gene&cmd=search&term=25526
Anxa1	0.577502	binding, bridging, enzyme inhibitor activity, lipid localization, lipid transport, protein binding, bridging, response to corticosteroid, response to estradiol, response to estrogen, response to glucocorticoid, skin development, structural molecule activity	http://www.ncbi.nlm.nih.gov/sites/entrez?db=gene&cmd=search&term=25380
C3	0.568421	acylglycerol metabolic process, blood coagulation, blood microparticle, coagulation, glycerolipid metabolic process, hemostasis, neutral lipid metabolic process, positive regulation of endocytosis, regulation of body fluid levels, response to corticosteroid, response to estradiol, response to estrogen, response to glucocorticoid, triglyceride metabolic process, wound healing	http://www.ncbi.nlm.nih.gov/sites/entrez?db=gene&cmd=search&term=24232
Ambp	0.538466	blood microparticle, enzyme inhibitor activity	http://www.ncbi.nlm.nih.gov/sites/entrez?db=gene&cmd=search&term=25377

Supplementary Table 9. Network explore of the significant eight genes.

Function	FDR	Genes in network	Genes in genome
response to estrogen	1.01E-05	8	248
extracellular matrix	1.01E-05	8	262
response to estradiol	1.01E-05	7	161
wound healing	1.35E-05	8	287
blood microparticle	1.35E-05	6	97
collagen	0.000131	4	26
collagen fibril organization	0.000399	4	35
regeneration	0.000403	6	184
structural molecule activity	0.000686	6	205
platelet-derived growth factor binding	0.000693	3	11
response to amino acid	0.000693	5	110
extracellular matrix part	0.000732	5	113
cellular response to amino acid stimulus	0.000767	4	47
triglyceride metabolic process	0.002934	4	67
proteinaceous extracellular matrix	0.002934	5	156
acylglycerol metabolic process	0.004191	4	75
neutral lipid metabolic process	0.004399	4	77
extracellular matrix structural constituent	0.004607	3	23
organ regeneration	0.008058	4	92
negative regulation of muscle cell apoptotic process	0.008552	3	29
growth factor binding	0.010201	4	100
skin development	0.011398	5	222
blood coagulation	0.013091	4	110
response to corticosteroid	0.013091	5	232
hemostasis	0.013515	4	112
coagulation	0.014445	4	115
regulation of body fluid levels	0.015354	5	246
blood circulation	0.016329	5	251
regulation of muscle cell apoptotic process	0.019955	3	43
lipid localization	0.024317	4	136
cellular response to acid	0.025657	4	139
muscle cell apoptotic process	0.026932	3	49
extracellular matrix organization	0.038657	4	157
extracellular structure organization	0.038657	4	158
protein binding, bridging	0.047688	3	61
lipid transport	0.053154	4	174
vagina development	0.055889	2	11
SMAD binding	0.060897	3	68
binding, bridging	0.063153	3	70
protein heterotrimerization	0.063153	2	12
killing of cells in other organism involved in symbiotic interaction	0.069923	2	13
disruption of cells of other organism involved in symbiotic interaction	0.069923	2	13
enzyme inhibitor activity	0.072136	4	197
positive regulation of endocytosis	0.086299	3	82
killing of cells of other organism	0.086299	2	15

glycerolipid metabolic process	0.086299	4	211
disruption of cells of other organism	0.086299	2	15
response to glucocorticoid	0.09548	4	218

Supplementary Table 10. Kyoto Encyclopedia of Genes and Genomes (KEGG) pathway enrichment analysis on MetaboAnalyst platform with 'Joint Pathway Analysis' mode.

Pathway name	Match status	p	-log(p)	Holm p	FDR	Impact
Arachidonic acid metabolism	2/82	0.00327	5.7229	0.69655	0.69655	0.05
Taurine and hypotaurine metabolism	1/9	0.009941	4.6111	1	0.93978	0.33333
Cardiac muscle contraction	1/12	0.013236	4.3248	1	0.93978	0.36364
Hypertrophic cardiomyopathy (HCM)	1/25	0.027411	3.5968	1	1	0.57143

Supplementary Table 11. Differentially expressed features by individual study and from meta-analysis.

	ID	BAT I	BAT II	BAT III	Combined Tstat	Combined Pval	Combined vip	Combined AUC
1	20cooh LTB4	-1.469	-1.866	-1.790	-83.112	1.220E-13	1.747	0.990
2	15-oxoETE	1.750	1.235	1.594	71.761	1.400E-11	1.390	0.911
3	15k PGF2a	1.703	-0.072	1.751	63.377	3.630E-10	1.412	0.981
4	LXB4	1.607	-0.457	1.575	53.991	1.940E-08	1.283	0.894
5	11bdhk PGF2a	1.402	-0.034	1.770	50.453	8.550E-08	1.436	0.971
6	6kPGF1a	1.556	0.232	-0.233	38.183	9.265E-06	1.658	0.829
7	5,15-diHETE	-0.665	-1.555	-1.084	-34.280	4.054E-05	1.366	0.924
8	8-iso PGF3a	-1.203	-1.169	-0.299	-33.891	4.620E-05	1.588	0.925
9	11-HEPE	1.030	1.546	-1.065	33.498	5.273E-05	1.230	0.843
10	PGB2	0.031	-1.828	-0.566	-33.413	5.273E-05	1.286	0.889
11	12-HEPE	-0.998	-1.434	0.162	-30.889	1.441E-04	1.487	0.940
12	PGF2a	0.806	1.515	0.289	29.857	2.059E-04	1.216	0.771
13	dihomo PGJ2	0.885	-1.527	-1.418	-29.465	2.294E-04	1.542	1.000
14	PGFM	1.006	1.388	-0.877	29.314	2.314E-04	1.348	0.870
15	Arachidonic	-0.837	1.784	-0.485	25.986	8.576E-04	1.015	0.869
16	15d PGD2	-0.640	-0.850	-1.204	-24.361	1.530E-03	1.376	0.905
17	2,3-dinor TXB2	-0.627	-1.263	-0.332	-21.719	3.817E-03	1.186	0.979
18	5,6-diHETrE	-0.517	-1.268	-0.443	-20.682	5.474E-03	1.374	0.918
19	PGA2	0.392	-1.618	0.006	-20.446	5.935E-03	1.000	0.750
20	20oh PGE2	-0.845	-0.243	-0.292	-16.965	0.020	1.172	0.854
21	dhk PGD2	-0.613	-0.240	-0.852	-16.264	0.025	1.310	0.866
22	PGJ2	0.521	0.670	-1.480	-14.545	0.045	1.613	0.750

(cut-off criterion: FC> 1.5 (OVX/con), p-value <0.05, AUC > 0.75, VIP > 1).

Supplementary Table 12. The phenotype, serum biochemistry analysis.

Protein quantification (n=3, mean ± s.e.m)	Urine Ptgds_ Peptides Ratio (Light/Heavy)_MRM	Uterus ERβ Fold change (ΔΔCT: 2-K)
Control_12 week	0.056±0.001	22.96±2.909
OVX_12 week	0.079±0.004**	4.61±0.618**

Organ/body weight ratio (%) (n=6, mean ± s.d.)	Body Weight (g)	Heart %	Liver%	Spleen%	Lung%	Kidney%	Uterus%	Brain%	Hypothalamus %	Hippocampus %
Control_12 week	297.12±16.66	0.33±0.02	3.58±0.21	0.22±0.01	0.56±0.05	0.76±0.04	0.37±0.11	0.72±0.04	0.043±0.013	0.047±0.004
OVX_12 week	360.22±15.04***	0.31±0.03NS	2.80±0.24***	0.19±0.04 NS	0.52±0.10 NS	0.623±0.04***	0.09±0.02***	0.66±0.05 NS	0.017±0.009**	0.047±0.002 NS

Biochemical Index	Kidney function profiles					Lipid profiles			
n=6, mean ± s.d.	ALB (g/L)	UA (μmol/L)	UREA (mmol/L)	GLU (mmol/L)	CREA (mmol/L)	TC (mmol/L)	TG (mmol/L)	HDL (mmol/L)	LDL (mmol/L)
Control_6 week	35.00±1.279	61.21±4.453	7.86±0.951	6.99±0.384	52.87±1.537	1.48±0.310	0.78±0.145	1.25±0.060	0.41±0.104
OVX_6 week	34.73±3.616	65.78±9.537	6.90±0.643	8.84±1.526*	63.13±1.102**	2.38±0.244**	1.23±0.279**	0.96±0.091**	0.50±0.051
Control_9 week	31.87±2.420	55.87±6.897	6.94±0.532	6.92±0.728	56.13±3.105	1.36±0.171	0.73±0.140	1.55±0.133	0.39±0.018
OVX_9 week	36.40±0.817**	63.62±8.757	8.87±0.695**	9.09±0.803**	60.9±2.578*	2.01±0.142**	1.39±0.140**	1.24±0.277*	0.58±0.116**
Control_12 week	30.02±1.072	66.23±6.028	6.49±1.053	6.81±0.357	59.73±3.075	1.75±0.365	0.61±0.199	1.86±0.019	0.49±0.072
OVX_12 week	33.32±1.606**	107.12±33.284*	8.83±0.972**	9.21±0.801**	65.33±3.554*	2.13±0.119*	1.47±0.409**	1.47±0.150**	0.67±0.091**

*p < 0.05, **p < 0.005, ***p < 0.0005 versus control rats. NS, not significant.

Please browse Full Text version to see the data of Supplementary Table 13

Supplementary Table 13. 'Gene-Metabolite-Phenotype' network analysis (urine & serum).

Supplementary Table 14. Western blot, immunohistochemistry and peptide MRM quantification results.

	Kidney		Uterus		Hypothalamus	
	ERβ	**Ptgds**	**ERβ**	**Ptgds**	**ERβ**	**Ptgds**
IF IOD/AREA score						
Control	0.0035±0.0003	0.0024±0.0004	0.0095±0.0009	0.0304±0.0007	0.0062±0.0003	0.0034±0.0004
OVX	0.0006±0.0001**	0.0087±0.0002***	0.0008±0.0001***	0.0024±0.0003***	0.0017±0.0006***	0.0011±6.849E-05*
OVX+E2	0.0032±0.0002$^{NS,\#\#}$	0.0034±0.0002 $^{NS,\#\#\#}$	0.0081±0.0006 $^{NS,\#\#\#}$	0.0296±0.0003 $^{NS,\#\#\#}$	0.0059±0.0002 $^{NS,\#\#\#}$	0.0032±9.231E-05 $^{NS,\#}$
WB assay						
Control	0.693±0.002	0.336±0.028	0.490±0.056	0.502±0.024	0.532±0.018	0.455±0.016
OVX	0.473±0.046***	0.536±0.023***	0.206±0.043***	0.189±0.022***	0.316±0.018***	0.244±0.036***
OVX+E2	0.629±0.011 $^{NS,\#\#}$	0.256±0.040 $^{NS,\#\#\#}$	0.525±0.024 $^{NS,\#\#\#}$	0.509±0.019 $^{NS,\#\#\#}$	0.488±0.015 $^{NS,\#\#}$	0.477±0.020 $^{NS,\#\#\#}$
PCR assay						
Control	0.47±0.099	1.27±0.176	22.96±2.909	0.380±0.010	114.237±9.776	180.137±4.688
OVX	0.057±0.027**	2.47±0.071***	4.61±0.618***	0.210±0.015***	44.137±1.979***	39.210±3.761***
OVX+E2	0.58±0.030 $^{NS,\#\#}$	1.35±0.060 $^{NS,\#\#\#}$	9.31±2.040 $^{*,\#\#}$	0.227±0.003 $^{*,\#\#}$	76.173±2.864 $^{*,\#\#}$	192.753±18.308 $^{NS,\#\#\#}$
Morris water maze						
	Escape latency (s)		Swimming distance to target (mm)		Times in target zone	
Control	5.850±2.011		1530.117±233.608		12.000±2.206	
OVX	25.767±6.110**		9791.883±1187.346***		2.667±0.494**	
OVX+E2	7.600±2.099 $^{NS,\#\#}$		2062.400±430.285 $^{NS,\#\#\#}$		8.833±1.682 $^{NS,\#}$	

(n=3, mean ± SEM).
$^{*}p < 0.05$, $^{**}p < 0.005$, $^{***}p < 0.0005$ versus control rats; $^{\#}p < 0.05$, $^{\#\#}p < 0.005$, $^{\#\#\#}p < 0.0005$ versus OVX rats. NS, not significant.